Atmos. Chem. Phys. Discuss., 9, 27485–27542, 2009
www.atmos-chem-phys-discuss.net/9/27485/2009/

Atmospheric Chemistry and Physics Discussions

This discussion paper is/has been under review for the journal Atmospheric Chemistry and Physics (ACP). Please refer to the corresponding final paper in ACP if available.

Elemental analysis of chamber organic aerosol using an aerodyne high-resolution aerosol mass spectrometer

P. S. Chhabra[1], **R. C. Flagan**[1,2], **and J. H. Seinfeld**[1,2]

[1]Division of Chemistry and Chemical Engineering, California Institute of Technology, Pasadena, CA, USA
[2]Division of Engineering and Applied Science, California Institute of Technology, Pasadena, CA, USA

Received: 3 December 2009 – Accepted: 4 December 2009 – Published: 21 December 2009

Correspondence to: J. H. Seinfeld (seinfeld@caltech.edu)

Published by Copernicus Publications on behalf of the European Geosciences Union.

Abstract

The elemental composition of laboratory chamber secondary organic aerosol (SOA) from glyoxal uptake, α-pinene ozonolysis, isoprene photooxidation, single-ring aromatic photooxidation, and naphthalene photooxidation is evaluated using Aerodyne high-resolution time-of-flight mass spectrometer data. SOA O/C ratios ranged from 1.13 for glyoxal to 0.30–0.43 for α-pinene ozonolysis. The elemental composition of α-pinene and naphthalene SOA was also confirmed by offline mass spectrometry. The fraction of organic signal at *m/z* 44 is generally a good measure of SOA oxygenation for all systems except for glyoxal uptake, in which *m/z* 44 substantially underpredicts O/C. Although chamber SOA has generally been considered less oxygenated than ambient SOA, single-ring aromatic- and naphthalene-derived SOA can reach O/C ratios upward of 0.7, well within the range of OOA, though still not as high as some ambient measurements. The spectra of aromatic- and isoprene-high-NO_x SOA resemble that of OOA, but the spectrum of glyoxal uptake does not resemble that of any PMF component.

1 Introduction

The chemical composition of secondary organic aerosol (SOA) from a volatile organic precursor comprises dozens of compounds owing to the variety of reaction pathways leading to semivolatile products (Hallquist et al., 2009; Kroll and Seinfeld, 2008). Offline analysis techniques can typically quantify only a portion of the wide array of compounds present in SOA. Though generally not able to provide detailed composition profiles of organic aerosol (OA), bulk, real-time mass spectrometric analysis has become an indispensable tool in chemically characterizing OA. The widely used Aerodyne quadrupole aerosol mass spectrometer (Q-AMS) uses thermal vaporization followed by electron impact ionization and a quadrupole mass analyzer to quantify the non-refractory portion of sub-micron aerosol mass (Jayne et al., 2000; Jimenez et al., 2003; Canagaratna et al., 2007). The original Q-AMS has been updated to improve sensitivity and time

ACPD

9, 27485–27542, 2009

resolution by replacing the quadrupole mass spectrometer with a compact time-of-flight mass spectrometer (C-ToF-AMS) (Drewnick et al., 2005). While the C-ToF-AMS does improve the mass resolution over the Q-AMS, it still does not effectively distinguish different ions with the same nominal mass. Large gains in mass resolution were achieved when a high-resolution time-of-flight mass spectrometer (H-TOF Series, Tofwerk, Thun, Switzerland) was combined with the original AMS design (HR-ToF-AMS) (DeCarlo et al., 2006). The advantage of the HR-ToF-AMS is that it can distinguish and quantify ions with the same nominal mass but different elemental compositions, e.g. organic ions of the form, $C_xH_y^+$, $C_xH_yO_z^+$, $C_xH_yN_p^+$, and $C_xH_yO_zN_p^+$, allowing for a more detailed analysis of the elemental composition of SOA, and most importantly, its oxygen content.

DeCarlo et al. (2006) demonstrated the first application of a field-deployable HR-ToF-AMS during the MIRAGE and SOAR-1 field campaigns and found that the vast majority of the organic signal could be attributed to either $C_xH_y^+$ or $C_xH_yO_z^+$ ions. Aiken et al. (2007) further developed HR-ToF-AMS analysis by showing that elemental ratios of OA, i.e. O/C, H/C, N/C and OM/OC, could be estimated from the relative intensities of chemically identified ion fragments. The first detailed analyses of high-resolution data was from the MILAGRO campaign measuring ambient aerosol in and around Mexico City (DeCarlo et al., 2008; Aiken et al., 2008, 2009). Aiken et al. (2008) demonstrated the first measurements of the elemental composition of ambient OA in this field campaign and showed that the O/C ratios ranged from 0.06–0.010 for primary organic aerosol (POA) to about 0.9 for the most oxidized aerosol. Aiken et al. (2008) also showed that the fraction of the *m/z* 44 signal to the total organic signal correlated well with O/C ratio and found it to be a good surrogate for the oxygen content of OA. DeCarlo et al. (2008) found that O/C ratios were highest in non-urban (regional) locations and that O/C could be a qualitative indicator of photochemical age. Aiken et al. (2008) performed the first positive matrix factorization (PMF) analysis on a HR-ToF-AMS data set from the MILAGRO campaign, finding that three components dominated OA: hydrocarbon-like organic aerosol (HOA, Avg. O/C=0.16), oxygenated

ACPD
9, 27485–27542, 2009

organic aerosol (OOA, Avg. O/C=0.60) and biomass burning organic aerosol (BBOA, Avg. O/C=0.30). A fourth factor from a local source with non-negligible nitrogen content was also found (LOA, Avg. O/C=0.13 and N/C=0.06). Recently, aerosol measurements were made at the peak of Whistler Mountain during INTEX-B and the average O/C was 0.83 (Sun et al., 2009). Thermal denuder measurements of OA from SOAR-1 and MILAGRO campaigns with a HR-ToF-AMS demonstrated that aerosol volatility was inversely correlated with O/C ratio (Huffman et al., 2009).

The first series of chamber laboratory experiments to which the HR-ToF-AMS elemental analysis was applied were of SOA generated from the photooxidation of α-pinene, isoprene, toluene, and gasoline vapors and ozonolysis of α-pinene. Analyzing data from these experiments, Aiken et al. (2008) concluded that chamber SOA, characterized by O/C ratios from 0.27–0.42, was less oxidized than ambient OOA (at concentrations higher than ambient, as used to derive the previous generation of SOA models). For α-pinene ozonolysis SOA, Shilling et al. (2009) demonstrated that the O/C ratio increased as aerosol loadings decreased, and at the lowest loadings, the mass spectrum resembled that of ambient OOA. Further work on the same system showed that a product specific volatility model could predict measured O/C ratios but overpredicted H/C ratios (Chan et al., 2009b). Mohr et al. (2009) also used the HR-ToF-AMS to measure the degree of oxygenation of POA from meat cooking, trash burning, and vehicle exhaust and concluded that emissions from such sources could not be a substantial source of ambient OOA. Other chamber studies have used the HR-ToF-AMS to study the chemical mechanism of SOA formation from specific precursors, such as glyoxal, naphthalene, and amines (Galloway et al., 2009; Chan et al., 2009a; Kautzman et al., 2009; Malloy et al., 2009). Most recently, the HR-ToF-AMS has been used to study the heterogeneous OH oxidation of squalane particles to infer the mechanisms of OA aging (Smith et al., 2009; Kroll et al., 2009).

Ambient studies with the HR-ToF-AMS infer that much of the oxygenation of OA occurs as a result of photochemical aging of SOA, with the highest O/C ratios measured in remote regions. PMF analysis of HR-ToF-AMS data identifies similar components to

ACPD
9, 27485–27542, 2009

those found from unit mass resolution data (Ulbrich et al., 2009; Zhang et al., 2005a,b, 2007; Lanz et al., 2007), the most common factors being HOA and OOA, which has been further subcategorized into low-volatility OOA (LV-OOA, previously known as OOA-1) and semi-volatile OOA (SV-OOA, previously known as OOA-2) (Jimenez et al., 2009). LV-OOA has been characterized as aged OOA, having O/C ratios upwards of 0.6 and spectra dominated by mass fragment CO_2^+ at *m/z* 44. Chamber SOA, however, generally does not exhibit as large O/C ratios as LV-OOA, at most reaching O/C ratios of SV-OOA and producing spectra with $C_2H_3O^+$ at *m/z* 43 as the dominant ion. In chamber investigations that use high precursor concentrations to generate SOA at aerosol loadings much higher than that of ambient OA, less oxygenated species partition into the particle phase. Additionally, chamber experiments are typically run for <24 h, which, while adequate to produce SOA from the photooxidation or ozonolysis of most SOA precursors, is still shorter than the atmospheric lifetime (~1 week) of ambient aerosol. Despite these limitations, chamber experiments are crucial to constraining SOA models and providing insight into the mechanisms involved in the formation and evolution of SOA (Kroll and Seinfeld, 2008). While comprehensive chamber studies of many different VOCs with the Q-AMS have been conducted (Bahreini et al., 2005), it has generally not been possible to directly compare offline speciation data to AMS data. The HR-ToF-AMS now provides the unique opportunity to make direct comparisons to offline speciation.

In this study we evaluate HR-ToF-AMS data on the elemental composition of chamber OA from a comprehensive suite of SOA systems: glyoxal uptake, α-pinene ozonolysis, isoprene photooxidation, single-ring aromatic photooxidation, and naphthalene photooxidation. We compare our findings to other laboratory composition studies and identify discrepancies and sources of uncertainty. In addition, we evaluate the use of *m/z* 44 as a surrogate for OA oxygenation. Lastly, we compare the elemental ratios measured in the chamber to those measured in ambient OA and derived from PMF analysis.

2 Experimental section

2.1 Chamber operation

All of the experiments analyzed here (Table 1) were performed in Caltech's dual 28 m^3 Teflon environmental chambers (Cocker et al., 2001; Keywood et al., 2004) over the period 2007–2009. Before each experiment, the chambers were flushed for > 24 h until the particle number concentration was <100 cm^3 and the volume concentration was < 0.1 m^3 cm^{-3}. Each chamber has a dedicated Differential Mobility Analyzer (DMA, TSI model 3081) coupled with a condensation nucleus counter (TSI model 3760) for measuring aerosol size distribution and number and volume concentration. Temperature, relative humidity (RH), ozone (O_3), NO, and NO_x were continuously monitored. For seeded experiments, ammonium sulfate seed particles were generated by atomization of a dilute aqueous ammonium sulfate solution using a constant rate atomizer.

For the experiments involving glyoxal, glyoxal preparation and experimental design are described by Galloway et al. (2009). Briefly, glyoxal uptake experiments begin by introducing gas-phase glyoxal into a dark, humid chamber and allowing the concentration to equilibrate over about 10 h. Approximately 160 ppb of cyclohexane was also added as a tracer for dilution. Once the gas-phase glyoxal concentration reached a steady state, ammonium sulfate seed aerosol was introduced and the resulting organic growth was monitored by both the DMA and HR-ToF-AMS. After organic growth leveled off, the chamber air mass was diluted with clean hydrocarbon-free air to investigate the reversibility of uptake. The amount of dilution was calculated by monitoring the cyclohexane concentration with a gas-chromatograph with flame ionization detector (GC-FID, Agilent 6890N).

Ozonolysis experiments are described by Chan et al. (2009b). The effect of humidity and H_2O_2 on SOA formation were tested and permutated in the four experiments. The parent hydrocarbon, α-pinene (50 ppb), and an OH scavenger, cyclohexane, were introduced separately by injecting known volumes of the liquid hydrocarbon into a glass bulb, subsequently carried into the chamber by an air stream at

5 L min^{-1}. The estimated mixing ratio of cyclohexane was 37 ppm, at which the rate of cyclohexane+OH exceeds that of α-pinene+OH by a factor of 100. O_3 injection was stopped after the O_3 concentration reached 180 ppb.

The protocol for isoprene (Kroll et al., 2006), single-ring aromatic (Ng et al., 2007), and naphthalene (Chan et al., 2009a) photooxidation experiments are described in detail in the references cited. For high-NO_x experiments (initial [NO]>300 ppb), nitrous acid (HONO) was used as an OH source, at amounts between 175 and 310 ppb. Additional NO was added until the total NO mixing ratio was about 400–500 ppb. For low-NO_x experiments, hydrogen peroxide (H_2O_2) was used as an OH source.

2.2 High-resolution time-of-flight aerosol mass spectrometer

In all of the experiments considered here, real-time particle mass spectra were collected continuously by a HR-ToF-AMS, henceforth referred to as the AMS (Canagaratna et al., 2007; DeCarlo et al., 2006). In the mode of operation, the AMS was switched once every minute between the high-resolution "W-mode" and the lower resolution, higher sensitivity "V-mode". The "V-mode" data were analyzed using a fragmentation table to separate sulfate, ammonium, and organic spectra and to time-trace specific mass-to-charge ratios (Allan et al., 2004). "W-mode" data were analyzed using a separate high-resolution spectra toolbox known as PIKA to determine the chemical formulas contributing to distinct mass-to-charge (*m/z*) ratios (DeCarlo et al., 2006).

The AMS elemental analysis procedure exploits the properties of electron impact (EI) ionization to determine the elemental composition of OA (Aiken et al., 2007). Briefly, the signal generated from the measured ion fragments of EI ionization is approximately proportional to the mass concentration of the initial species (Jimenez et al., 2003; Crable and Coggeshall, 1958). Because HR-MS can determine the chemical formula of each ion fragment, the average elemental composition of all ions can be calculated.

Thus the relative mass concentration M_X of a given element X is computed as follows:

$$M_X = \sum_{i=m/z_{\min}}^{m/z_{\max}} I_i \frac{m_X}{m_i} \quad (1)$$

where I_i is the ion signal at fragment i, m_X is the atomic mass of element X, and m_i is the mass of fragment i. The elemental ratio X/Y is then

$$X/Y = \alpha_{X/Y} \frac{\frac{M_X}{m_X}}{\frac{M_Y}{m_Y}} \quad (2)$$

where $\alpha_{X/Y}$ is the calibration factor for that particular ratio, determined by laboratory samples with known elemental compositions. The organic mass to organic carbon ratio OM/OC ratio is calculated as follows

$$\mathrm{OM/OC} = \frac{12 + (16 \times \mathrm{O/C}) + (1 \times \mathrm{H/C}) + (14 \times \mathrm{N/C}) + \ldots}{12} \quad (3)$$

Aiken et al. (2007, 2008) sampled 59 different standards with the HR-ToF-AMS and determined calibration factors for O/C, H/C, and N/C and estimated uncertainties for each ratio as shown in Supplemental Table S1: http://www.atmos-chem-phys-discuss.net/9/27485/2009/acpd-9-27485-2009-supplement.pdf. O/C, H/C, N/C and OM/OC ratios in the present study were computed using the computation toolbox "Analytical Procedure for Elemental Separation" (APES), which applies the analysis procedure as described Aiken et al. (2007, 2008) to the W-mode data.

O/C ratios were also estimated from V-mode data using the organic signal at *m/z* 44 (with gas-phase CO_2 signal removed) as a surrogate for oxygenation in OA. Typically, the *m/z* 44 signal arises from CO_2^+ ions, which are commonly formed from the fragmentation of carboxylic acids (Takegawa et al., 2007). Aiken et al. (2008) correlated the fraction of organic signal at *m/z* 44 to the O/C ratio determined from HR-AMS data and derived the following empirical relationship based on Mexico City Data

ACPD
9, 27485–27542, 2009

$$O/C_{44} = 3.82 \times f_{44} + 0.0794 \quad (4)$$

where O/C_{44} is the estimated O/C ratio using *m/z* 44 as a surrogate and f_{44} is the organic signal at *m/z* 44 divided by the total organic signal. To distinguish between the O/C ratios determined from V- and W-mode data, the O/C ratio calculated from *m/z* 44 from V-mode data will be referred to as O/C_{44}, and the O/C ratio determined from W-mode data in APES will be referred to as O/C_{HR} when the two are compared.

APES allows for special treatment of ions that may have contamination from air and allows users to include "ion families" that are traditionally considered fragments of inorganic species as part of the organic mass. The CO_2^+ signal originating from ambient air CO_2 is removed to determine the organic signal at *m/z* 44. Fourier transform infrared spectroscopy measurements show the concentration of CO_2 in the chamber air is nominally the same as in the atmosphere, estimated to be 370 ppm. The ion CO^+ (*m/z* 28) signal, another common fragment of organic species, tends to be overwhelmed by N_2^+ from N_2 in ambient air. As a result, the contribution of CO^+ to the total organic signal is usually estimated as a factor of the CO_2^+ organic signal. The ratios of the particle-phase signals of CO^+ to CO_2^+ are listed in Supplemental Table S2: http://www.atmos-chem-phys-discuss.net/9/27485/2009/acpd-9-27485-2009-supplement.pdf and were determined from HR spectra of experiments in which the OA loading is high, for all systems except isoprene photooxidation, for which the default ratio was used. The signals from H_2O^+, OH^+, and O^+ in the particulate organic mass may suffer interference from gas-phase H_2O, and their organic contributions are estimated as suggested in Aiken et al. (2008). For all experiments, ions in the "OH family" that are not H_2O^+, OH^+, and O^+ are added as part of the organic mass; however, their inclusion turns out to be negligible to the O/C and H/C calculations.

Particulate nitrogen signals were observed in high-NO_x photooxidation experiments, mostly originating from NO^+ and NO_2^+ ions. In ambient studies, these ions usually result from the fragmentation of inorganic nitrates in the particle phase. Although gas-phase nitric acid is produced from the $OH+NO_2$ reaction, at low chamber humidities,

nitric acid is not expected to partition appreciably into the particle phase. Thus, the signals of NO^+ and NO_2^+ ions, termed as "NO Family" ions, are included as part of the organic mass in high-NO_x photooxidation experiments to estimate the contribution of nitrogen from organonitrate compounds.

3 Results

Table 2 lists the average elemental ratios at the time of the peak O/C ratio for each experimental system. Aerosol produced from glyoxal uptake exhibits the largest average O/C and OM/OC at 1.13 and 2.68, respectively, and α-pinene-O_3 SOA has the smallest average O/C and OM/OC at 0.43 and 1.70, respectively. SOA from all OH-photooxidation experiments exhibits intermediate O/C and OM/OC values ranging from 0.57 to 0.74 and 1.89 to 2.15. Values of N/C are essentially zero for low-NO_x experiments and do not exceed 0.08 for high-NO_x experiments. Values of H/C vary from 1.39 to 1.64 for all systems except naphthalene-OH, which is 0.89 on average. Time trends of O/C, H/C and OM/OC ratios for systems with the same VOC and NO_x conditions largely overlap, illustrating that elemental ratios tend to be a function of the extent of conversion of the parent hydrocarbon. OM/OC follows the same time dependence as O/C, as oxygen is the only major source of SOA mass other than carbon.

3.1 SOA from reactive uptake of glyoxal

Recently, glyoxal has received attention as being a possible ambient SOA precursor. It has been estimated that glyoxal could contribute to at least 15% of the SOA formation in Mexico City (Volkamer et al., 2007) and has been implicated in SOA formation from the photooxidation of acetylene (Volkamer et al., 2009). As we will show, the O/C ratio of glyoxal-SOA determined in the laboratory is the largest of any system we consider. Dzepina et al. (2009) modelled SOA formation in Mexico City, including glyoxal SOA, as well as updated aromatic SOA yields and SOA from primary semivolatile and

intermediate volatility species. To evaluate the model, they compared the predicted O/C ratios to those measured in Mexico City; assuming an O/C ratio of 0.37 for aromatic SOA (Aiken et al., 2008), the model underpredicts the oxygen content of the ambient aerosol. When glyoxal is included as an SOA constituent and assumed to have an O/C of 1.0, the modelled SOA O/C is in much closer agreement with ambient measurements (while the assumed O/C of glyoxal is close to what we will report below, the O/C assumed for aromatic SOA is considerably lower than that measured).

Figure 1 displays the time dependence of OM/OC, H/C, O/C, and N/C ratios during the three glyoxal uptake experiments. At the onset of uptake, O/C and OM/OC rise sharply, reaching values of 1.13 and 2.68, respectively, the largest of these ratios of all the systems studied. This is not unexpected as pure glyoxal itself has an O/C of 1 and OM/OC of 2.42, the highest of all the VOCs investigated. In aqueous solution, the two aldehyde groups of glyoxal can be hydrated, adding two H_2O molecules. Also, glyoxal can polymerize to aldols and acetals, removing H_2O (Whipple, 1970; Fratzke and Reilly, 1986; Loeffler et al., 2006). Thus, the O/C of aqueous-phase glyoxal can be as high as 2, H/C as high as 3, and OM/OC as high as 3.92. The measured ratios lay between these bounds, suggesting that both hydration and polymerization processes are occurring in the wet ammonium sulfate seed.

One can estimate the extent of polymerization based on the elemental composition measured by the AMS. Assuming that free glyoxal in the particle phase is hydrated twice, $C_2H_2O_2 \cdot 2H_2O$, and that oligomerization produces straight chain acetals, for every monomer unit added to the chain, two water molecules are lost. Thus, a glyoxal oligomer will have the formula $C_{2n}O_{2n+2}H_{2n+4}$ where n is the number of glyoxal subunits. On this basis, one gets O/C=$(n+1)/n$, H/C=$(n+2)/n$, and OM/OC=$(29n+18)/12n$. Using the elemental values in Table 2 and solving for n, the number of glyoxal subunits ranges from 4 to 8. Kua et al. (2008) performed DFT calculations to study the aqueous phase hydration and oligomerization of glyoxal and found that the dioxolane ring dimer ($C_4H_8O_6$, O/C=1.5, H/C=2, OM/OC=3.2) is the preferred thermodynamic form for oligomerization and that the

hydrated trimer ($C_6H_{10}O_8$, O/C=1.3, H/C=1.7, OM/OC=2.9) is the oligomer endpoint. These structures imply a smaller extent of oligomerization than suggested by the AMS elemental ratios. The AMS analysis technique may be underestimating the organic oxygen in the glyoxal/$(NH_4)_2SO_4$(aq) system but is within the reported measurement uncertainty of about 31% (Table S1: http://www.atmos-chem-phys-discuss.net/9/27485/2009/acpd-9-27485-2009-supplement.pdf).

Figure 2a shows the contribution of each *m/z* to the elemental composition of the organic mass at the peak of organic growth. About 56% of the signal comes from CHO^+, CH_2O^+, and CH_3O^+ fragments at *m/z* 29-31, with smaller contributions from $CH_3O_2^+$, $C_2H_2O_2^+$, $C_2H_3O_2^+$, and $C_2H_4O_2^+$. Together, these ions represent the bulk of the oxygen signal in the AMS spectra. As identified by Galloway et al. (2009), other distinct fragments that appear in the spectrum, $C_4H_7O_5^+$, $C_5H_5O_5^+$, and $C_6H_7O_6^+$, suggest the existence of oligomers of at least n=3. About 1% of the total AMS signal can be attributed to nitrogen-containing organic fragments resulting from the reaction of glyoxal with ammonium, producing imidazoles (Galloway et al., 2009). Signals from the fragmentation of these compounds result in a measured N/C ratio for this system of about 0.01. This is possibly an underestimate of the organic nitrogen signal as imidazoles may fragment into NH_x^+ ions. These ions are part of the "NH family" of ions and were not included as part of the organic signal since they are the primary fragments of ammonium in the ammonium sulfate seed.

After organic growth by glyoxal uptake had ceased in experiments 1 and 2, the chamber was diluted with clean air to investigate the reversibility of glyoxal uptake. As shown in Fig. 1, aerosol O/C decreases slowly after dilution, H/C stays approximately constant, and N/C increases gradually. The AMS organic signal and glyoxal markers decrease relative to sulfate during dilution, showing that glyoxal can repartition to the gas phase and that uptake is reversible (Galloway et al., 2009). Also, markers for N-containing compounds presumably formed from the reaction of glyoxal and ammonium, such as 1H-imidazole-2-carboxaldehyde ($C_4H_4N_2O$, O/C=0.25, H/C=1, N/C=0.5), increase relative to sulfate. These N-containing compounds are formed as ammonia

replaces H_2O as part of the organic phase, decreasing O/C and increasing N/C.

3.2 *α*-pinene ozonolysis SOA

The elemental and OM/OC ratios for the four *α*-pinene/O_3 SOA experiments evaluated here are similar so only data from experiment 4 are discussed. Figure 3 shows the evolution of OM/OC, H/C and O/C ratios of the SOA for experiment 4. The earliest aerosol formed has an O/C ratio of 0.50, which decreases throughout the experiment to approximately 0.30, close to the O/C ratio reported by Aiken et al. (2008) for this system. The H/C ratio increases from about 1.3 to 1.5. These ratios are in good agreement with the high-resolution AMS measurements of Shilling et al. (2009). This behavior has been explained by increased partitioning of less oxidized semivolatile compounds as the mass of partitioning medium grows (Shilling et al., 2009; Chan et al., 2009b). There is no substantial difference in SOA elemental composition between humid and dry experiments and experiments with and without H_2O_2.

α-Pinene ozonolysis has served as a canonical SOA system for which the particle-phase composition of *α*-pinene SOA has been investigated in numerous studies (Yu et al., 1999; Jang and Kamens, 1999; Glasius et al., 2000; Koch et al., 2000; Iinuma et al., 2004; Gao et al., 2004). Using a denuder/filter pack sampling system and derivatization with GC-MS detection, Yu et al. (1999) were able to identify >90% of the aerosol composition by mass at the molecular level. Using the molar yields reported in Yu et al. (1999), we calculate the aerosol-phase elemental ratios for their *α*-pinene/O_3 experiments as shown in Supplemental Table S3: http://www.atmos-chem-phys-discuss.net/9/27485/2009/acpd-9-27485-2009-supplement.pdf. The composition analysis yields an O/C range of 0.34–0.36 and an H/C range of 1.56–1.58, which are very close to the AMS measured values. Using the Nanoaerosol Mass Spectrometer, Tolocka et al. (2006) determined the aerosol products of *α*-pinene/O_3 to have an O/C ratio of 0.37 to 0.4 for nucleated particles 30 and 50 nm in diameter. Reinhardt et al. (2007) used filter sampling in conjunction with electrospray ionization mass spectrometry to determine O/C ratios of 0.4

to 0.6. A comparison of the elemental analyses in this work and others is given in Table 3.

Important ions in the α-pinene/O_3 system are noted in Fig. 2b, with the largest contribution to the total organic signal coming from $C_2H_3O^+$ (*m/z* 43) and the largest contribution to oxygen coming from CO_2^+ (*m/z* 44) at the peak of organic loading. Other prominent peaks reported by Shilling et al. (2009) are also observed. Over the course of the experiments evaluated here, the contribution of *m/z* 44 to the organic signal decreases from approximately 11% to 6–7% as the organic mass increases.

3.3 Isoprene SOA

3.3.1 Low-NO_x

Figure 4 tracks the organic growth, isoprene decay, and elemental ratios for experiment 10, the longest duration experiment conducted under low-NO_x conditions. The SOA mass peaks soon after the onset of irradiation but then decreases rapidly. Kroll et al. (2006) suggested that the rapid loss in organic mass could be attributed to photolysis of semivolatile or condensed-phase hydroperoxides, as the decay occurred only under irradiation and only in a low-NO_x environment. This hypothesis was supported by Surratt et al. (2006) who found, using iodometric-spectrophotometric measurements, that the contribution of organic peroxides decreased from 59% of the total SOA mass to 26% over the 12 h duration.

For low-NO_x isoprene SOA, the O/C ratio is approximately 0.60 at the onset of photooxidation, decreasing gradually to 0.50 in the longest duration experiment. The H/C ratio starts at approximately 1.2, increases to 1.6, and then steadily decreases to 1.45. Using offline filter analyses, several classes of compounds have been identified as constituents of SOA from the photooxidation of isoprene under low-NO_x conditions with ammonium sulfate seed, including dihydroxydihydroperoxides (O/C=1.2, H/C=2.4), epoxydiols (O/C=0.6, H/C=2), C_5-alkene triols (O/C=0.6, H/C=2), 2-methyltetrols (O/C=0.8, H/C=2.4), and hydroxyl sulfate esters (O/C=1.4, H/C=2.4, S/C=0.2) (Claeys

et al., 2004; Wang et al., 2005; Surratt et al., 2006, 2007; Gómez-González et al., 2008; Surratt et al., 2009). Oligomers of 2-methyltetrols and hydroxy sulfate esters have also been measured (Surratt et al., 2006, 2008). An O/C value of 0.6 is consistent with SOA consisting of epoxydiols and C_5-alkene triols. However, numerous studies have reported peroxides and 2-methyltetrols as major constituents as well, both having higher degrees of oxygenation. Tetrol dimers and sulfate esters will also have O/C ratios higher than 0.6. Therefore, the expected particle-phase composition of isoprene-OH SOA has higher O/C and H/C ratios than those measured by the AMS, reasons for which will be discussed in Sect. 4.2. However, the slow decay of the O/C ratio over time could reflect the photolysis of hydoxyhydroperoxide compounds or reaction with OH radicals (Lee et al., 2000). Photolysis would split the peroxy bond, releasing an OH radical. The subsequent alkoxy radical would then react with O_2 to form an aldehyde and HO_2. Reaction with OH would abstract a hydrogen leaving an alkoxy peroxy radical which could then further decompose. Overall these processes have the potential to deplete both oxygen and hydrogen relative to carbon, reducing their elemental ratios.

The time dependence of the H/C ratio is consistent with the effects of two different processes. H/C rises quickly to a peak at about 200 min into the experiment, coinciding with the peak of SOA growth. The increasing amount of OA provides a medium for continued partitioning of semivolatile species with a higher H/C ratio into the particle phase. This effect is also seen in the H/C ratio of α-pinene ozonolysis SOA. However, as noted earlier, with continued irradiation, peroxide compounds could photolyze or react with OH, causing the H/C ratio to decrease. The decrease in H/C and O/C ratios could also be explained by oligomerization, as H_2O is lost through condensation reactions.

The spectrum of low-NO_x isoprene SOA changes throughout irradiation time reflecting the continued processing of the SOA, consistent with the observed rapid decay in organic aerosol mass. At the peak of aerosol growth about 85% of the organic signal occurs for $m/z \leq 45$. The strongest signals occur at COH^+ and $C_2H_3O^+$, representing approximately 30% of the organic signal as displayed in Fig. 5a, with most of the

oxygen content coming from COH^+. The spectrum changes considerably after 20 h of irradiation with the contribution of the organic signal decreasing to 75% for $m/z \leq 45$ and contributions of $m/z > 100$ increasing. Mass fragment CO_2^+ also becomes the dominant contributor of oxygen to the SOA. Unit-mass resolution AMS data from Surratt et al. (2006) indicate an increasing signal at $m/z > 200$ over the course of the experiment, suggesting oligomerization even as organic mass is decreasing. The authors of this previous study also proposed m/z 91 as an AMS tracer ion for peroxides, as the ion reaches its peak signal earlier than that of organics and decreases faster than wall loss. The high-resolution study here confirms the existence of their ion assignment of $C_3H_7O_3^+$, though it also occurs with $C_7H_7^+$.

3.3.2 High-NO_x

Under high-NO_x conditions, isoprene SOA is characterized by O/C atomic ratios generally higher than those of low-NO_x experiments. As illustrated in Fig. 6, H/C, O/C and OM/OC ratios quickly plateau to 1.46, 0.62, and 2.00, respectively, and do not change over the course of the experiments. The N/C ratio, however, peaks early at approximately 0.05 and decreases thereafter. Figure 7 compares the organic growth and isoprene decay to the O/C ratio, and the gas-phase NO and NO_2 concentrations to the N/C ratio for experiment 12, conducted under high-NO_x conditions. In contrast to low-NO_x experiments, as the isoprene concentration drops, organic mass grows to a plateau about 4 h after irradiation begins. After organic growth levels out, additional HONO is added to convert any existing gas-phase intermediates such as methacrolein and peroxymethacroyl nitrate (MPAN) (Surratt et al., 2009); additional SOA is formed but no change in elemental composition is observed.

Previous work has established that the main constituents of SOA derived from isoprene photooxidation under high-NO_x conditions are 2-methylglyceric acid (O/C=1, H/C=2), the hydroxynitrate of 2-methylglyceric acid (O/C=1.75, H/C=1.75, N/C=0.25), and their corresponding oligoesters (Surratt et al., 2006, 2009; Szmigielski et al., 2007) from detailed offline chemical analyses of filter samples. Thus the AMS elemental ratios

are below those that would be expected from offline filter analysis. Even if one considers the linear oligomerization of 2-methylglyceric acid by esterification, which will reduce the O/C and H/C ratios by removing H_2O, the O/C ratio will not fall below 0.75 and the H/C ratio will not fall below 1.5.

SOA derived from isoprene photooxidation under high-NO_x conditions also has non-negligible nitrogen content. The nitrogen is likely organic in nature as the gas-phase concentration of NO_2 remains high throughout the experiment (Fig. 7), and recent work has shown that a major route to form isoprene-SOA under high-NO_x conditions occurs through the reaction of the methacrolein peroxy radical with NO_2 to form MPAN (Surratt et al., 2009). Aerosol-phase compounds containing nitrogen are presumably the hydroxynitrate of 2-methylglyceric acid or nitroxypolyols, which fragment in the AMS forming NO^+ and $NO_2{}^+$ ions (Fig. 5b). While the addition of extra HONO produces more SOA, it does not alter the elemental ratios, and continued irradiation led to no measurable aerosol processing (Fig. 7). If the aerosol-phase nitrogen resulted from the uptake of HNO_3, one would expect a jump in the N/C ratio with the second addition of HONO, just as in the beginning of the experiment. The N/C ratio decreases throughout the experiment, which could be the result of hydrolysis of the aerosol-phase organonitrates to form volatile nitric acid (Sato, 2008), or photolysis to form an alkoxy radical and NO_2 (Renbaum and Smith, 2009; Roberts and Fajer, 1989). The steady oxygen and hydrogen content of the isoprene high-NO_x SOA is supported by the relatively constant HR spectra. In contrast to the low-NO_x isoprene SOA spectrum (Fig. 5a), much of the oxygen in the high-NO_x AMS spectrum comes from $CO_2{}^+$.

3.4 Single-ring aromatic SOA

Figure 8 shows the O/C, H/C, N/C and OM/OC ratios for single-ringed aromatic SOA experiments (i.e., *m*-xylene and toluene). Maximum O/C ratios ranged from 0.60 to 0.73. Toluene SOA under high-NO_x conditions achieves an O/C of about 0.7. Low-NO_x

ACPD
9, 27485–27542, 2009

experiments begin with low O/C values that increase with continued irradiation. The O/C of high-NO_x SOA increases with continued irradiation as well, albeit more slowly. The N/C ratio of high-NO_x SOA peaks at 0.10 shortly after irradiation begins, but decreases gradually throughout the experiment.

While numerous studies have investigated the chemical composition of SOA from toluene photooxidation, as well as other aliphatic aromatic compounds, usually in the presence of NO_x, quantification of particle-phase organic species has proved difficult (Hamilton et al., 2005; Sato et al., 2007). Kalberer et al. (2004) found that a large fraction of the SOA formed from trimethylbenzene was oligomeric; proposed polymer structures lead to an O/C ratio of 1.0, and peaks from LDI-MS spectra have O/C ratios ranging from 0.7 to 1.6. For the same system, Fisseha et al. (2004) found that organic acids constitute 20 to 45% of the organic mass. If one considers the small organic acids quantified by Fisseha et al. (2004), O/C ratios would range from 1 to 2, substantially higher than those measured in the experiments surveyed here. Furthermore, aromatic photooxidation yields considerable amounts of glyoxal, methylglyoxal, and other multifunctional carbonyls that, if incoporated into the SOA, would produce high O/C ratios (Bloss et al., 2005; Hamilton et al., 2005, 2003; Kalberer et al., 2004). However, with the number of less oxygenated compounds measured, including aromatic ring-retaining compounds, unsaturated acids, ketones and aldehydes (Sato et al., 2007; Hamilton et al., 2005; Jang and Kamens, 2001), the measured O/C could accurately represent the oxygen content of the SOA formed.

AMS data indicate that *m*-xylene-derived SOA has a lower O/C ratio than that of toluene SOA. This is likely due to the presence of the second methyl group in *m*-xylene. For both NO_x conditions and hydrocarbons, the O/C ratio continues to increase over the course of oxidation, indicating continued oxidation of the aerosol even after the organic loading has peaked. This prolonged processing, perhaps as a result of OH oxidation of unsaturated compounds in the particle phase or of vapor-phase semivolatile species, leads to a greater contribution of CO_2^+ to the organic signal in each experiment. The SOA from both high-NO_x experiments had similar N/C ratios.

ACPD
9, 27485–27542, 2009

Under high-NO_x conditions, organic nitrogen as evidenced by the presence of (Hamilton et al., 2005; Sato et al., 2007; Jang and Kamens, 2001). Compounds, like nitrocresols and nitrotoluenes, form from the reaction of the OH-aromatic adduct with NO_2, which under high-NO_x conditions has the same concentration profile as in Fig. 8. N/C decreasing could reflect the continued photoooxidation of these compounds in the gas or particle phases.

At the peak of SOA growth, toluene SOA exhibits similar spectra regardless of NO_x level (Fig. 9), except for the existence of the NO^+ and $NO_2{}^+$ ions in high-NO_x spectra. Mass fragment $CO_2{}^+$ contributes nearly the same amount to the organic signal as $C_2H_3O^+$ in toluene experiments. Conversely, $C_2H_3O^+$ is the dominant ion in *m*-xylene SOA spectra, representing 19% of the organic signal in low-NO_x conditions and 15% in high-NO_x conditions (Fig. 9). In both systems, the fraction of $CO_2{}^+$ increases with continued irradiation.

3.5 Naphthalene SOA

Figures 11 and 12 show the elemental ratios for SOA derived from naphthalene photooxidation at high- and low-NO_x conditions, respectively. O/C ratios under low-NO_x conditions decrease sharply to 0.30 early in the experiments, but then increase to above 0.70 in the longest experiment. H/C ratios decrease from approximately 1.0 to 0.9. O/C and H/C ratios for high-NO_x experiments exhibit similar characteristics; O/C ratios start from about 0.35 at the beginning of irradiation and then increase steadily to 0.60 in the longest experiment, but no initial decrease occurred. H/C ratios decrease from 1.0 to approximately 0.8. N/C profiles under high-NO_x conditions resemble those of isoprene and aromatic high-NO_x systems, starting high at 0.10 and decreasing with continued irradiation. Figure 14 show the spectra for SOA derived under both NO_x levels.

The elemental values measured by the AMS are close to those determined in a comprehensive study of naphthalene photooxidation by Kautzman et al. (2009), who characterized, from detailed offline chemical analyses of filter samples, 68% and

53% of the SOA mass under low-NO_x and high-NO_x conditions, respectively. Acidic species and peroxides represented a major portion of the SOA in both NO_x regimes, and nitrogen-containing constituents were 3% of the total SOA mass formed under high-NO_x conditions. The O/C and H/C ratios calculated in that study were 0.50 and 0.82 under low-NO_x conditions and 0.51 and 0.83 under high-NO_x conditions. The N/C ratios measured by the AMS varied from 0.02 to 0.10 for SOA formed at high-NO_x conditions, in good agreement with Kautzman et al. (2009), as they estimate a lower bound estimate of N/C to be 0.04 from filter techniques.

Under low-NO_x conditions, O/C values descend slightly within the first hour of irradiation, which is likely a result of less oxygenated species partitioning into the growing organic phase. This phenomenon is not observed in the high-NO_x case, presumably because the high rates of oxidation and aerosol growth obscure this effect. As in the single-ringed aromatic experiments, the O/C ratio of naphthalene-derived SOA increases well after the organic mass has reached a maximum in both NO_x regimes (Fig. 13). This behavior is consistent with continued OH oxidation of semivolatile species, since most of the gas- and aerosol-phase species still retain aromaticity and unsaturation that are susceptible to oxidation by OH. Under high-NO_x conditions, the rapid decline of N/C could explained by photolysis of nitrogen containing compounds (Atkinson et al., 1989; Kautzman et al., 2009).

4 Discussion

4.1 Overall trends in O/C ratios from laboratory chamber-generated SOA

Of the VOCs studied here, glyoxal is unique because no oxidant initiates SOA formation. Based solely on its vapor pressure, glyoxal, the smallest dicarbonyl, would not be expected to produce SOA . Due to its ability to hydrate and polymerize, however, glyoxal has a large effective Henry's law constant (Loeffler et al., 2006; Ip et al., 2009).

These properties, along with its small carbon number, lead to the largest O/C of any system studied here and a measured O/C ratio greater than 1.

Although α-pinene along with naphthalene, has the highest carbon number, it produced the least oxygenated SOA. This is because, with 10 carbons, α-pinene has only one double bond, that is the only active site for ozone reaction. The lack of subsequent ozonolysis reactions limit oxygenation to first-generation products, primarily consisting of oxocarboxylic acids, dicarboxylic acids, and hydroxyl pinonic acid (Yu et al., 1999). This is supported by the chamber AMS data reported by Ng et al. (2006), which shows that the SOA chemistry is virtually constant over time. AMS elemental analysis confirms this as O/C and H/C ratios remain unchanged after semivolatile partitioning has reached equilibrium.

Like single-ringed aromatic SOA, the O/C ratios of naphthalene SOA increase with irradiation time, surpassing 0.7 for the longest low-NO_x experiments. The aromaticity of naphthalene, toluene, and *m*-xylene allow for multiple oxidation steps through ring opening and bicyclic peroxy radical routes (Kautzman et al., 2009; Bloss et al., 2005; Alvarez et al., 2007). The different rates of O/C ratio growth between high- and low-NO_x conditions can be explained by the source of OH radicals. Under high-NO_x conditions, the rapid photolysis of HONO yields high concentrations of OH radicals ($\sim 3\times10^7$ molecules cm^{-3}) at the onset of irradiation, which promptly generates SOA. SOA growth slows once HONO is consumed and OH radicals are produced through NO_x/HO_x cycling. Thus, under high-NO_x conditions, O/C ratios for naphthalene and single-ringed aromatic-SOA start high, and then increase slowly afterward, as depicted in Fig. 13. Under low-NO_x conditions, ppm levels of H_2O_2 are needed to reach an adequate OH concentration and OH levels are lower ($\sim 3\times10^6$ molecules cm^{-3}) but more constant throughout the experiment. O/C ratios of the earliest formed low-NO_x SOA are lower than in the high-NO_x case, but grow steadily throughout.

Of the 5 carbons of isoprene, four are subject to OH attack, leading to higher O/C ratios that SOA from α-pinene ozonolysis. Isoprene photooxidation yields very different SOA products depending on the NO_x level. Under low-NO_x conditions, isoprene

photooxidation products consist predominantly of polyols and peroxides (Surratt et al., 2006, 2009). These compounds initially give isoprene-SOA high O/C values, but due to photolysis or oligomerization reactions, the O/C ratio decreases. This behavior is in contrast to the behavior of single-ringed aromatic and naphthalene-SOA, in which the O/C ratios tend to increase with time. SOA from isoprene photooxidation under high-NO_x conditions is predominantly comprised of 2-methylglyceric acid and its corresponding oligoesters (Surratt et al., 2006, 2009; Szmigielski et al., 2007). However, O/C and H/C ratios remain constant over the course of oxidation.

4.2 Comparisons with offline analytical techniques

The elemental ratios measured by the HR-ToF-AMS can be compared to those of compounds detected by offline analytical techniques, such as coupled chromatography/mass spectrometry of filter extractions. For systems for which the majority of the SOA mass can be quantified by offline advanced analytical techniques, the elemental composition of both measurement techniques can be compared and validated. For α-pinene/O_3 and naphthalene photooxidation SOA, a substantial portion of the total organic mass has been identified and quantified by coupled gas or liquid chromatography/mass spectrometry (GC/MS or LC/MS) methods (Yu et al., 1999; Kautzman et al., 2009). Mole-weighted calculations of H/C, O/C and N/C ratios of the quantified species in those systems are very close to the measured elemental composition of the HR-ToF-AMS. In contrast, quantification of many of the particle-phase constituents of isoprene, toluene, and *m*-xylene photooxidation in both NO_x regimes has been difficult to achieve. For isoprene photooxidation, Surratt et al. (2006) were able to quantify roughly 20% of the SOA mass formed under high-NO_x conditions and 30% under low-NO_x conditions. These measurements, however, have associated uncertainties. Because exact standards were not available, acidic species formed under high-NO_x conditions were quantified using surrogate standards. In addition, peroxides formed under low-NO_x conditions were quantified using a surrogate with a molecular weight close to the

average molecular weight determined from mass spectrometry techniques. Quantification of compounds in aromatic-SOA has been difficult as well, though much of the mass has been attributed to small organic acids (Kalberer et al., 2004; Fisseha et al., 2004). Despite the lack of mass closure, the elemental ratios determined by the HR-ToF-AMS can be compared to the compounds identified from these speciation studies. As noted earlier, the AMS-derived O/C ratios of isoprene and aromatic SOA tend to be lower than those of representative compounds identified by coupled chromatography/mass spectrometry. One possible reason for this difference is the extensive oligomerization present in the particle phase of both systems. Isoprene-SOA formed under both low- and high-NO_x conditions has been found to form high-MW compounds, either by oligomerization or organosulfate formation (Surratt et al., 2006, 2007, 2009; Szmigielski et al., 2007). For example, Surratt et al. (2006) estimated that 2-methylglyceric acid and its corresponding oligoesters comprise 22–34% of the high-NO_x SOA mass. In addition, Kalberer et al. (2004) found that about 50% of the trimethylbenzene SOA mass was oligomeric, possibly from the particle-phase reactions of small acids (Fisseha et al., 2004). Esterification, aldol condensation, and hemiacetal/acetal formation reactions have been implicated in producing oligomers. Esterification and aldol condensation reactions, however, release H_2O which can evaporate to the gas-phase which may occur under low RH conditions. Through VTDMA measurements, Dommen et al. (2006) found that under dry conditions, isoprene SOA volatility is suppressed, implying an enhancement of oligomerization at lower relative humidity. Removal of H_2O will give lower O/C and H/C ratios measured by the AMS when compared to the monomers measured detected through chromatography. Substantial oligomerization has also been observed in α-pinene/O_3 SOA by Gao et al. (2004); however, the relatively low oxygenation of the SOA likely restrains condensation reactions. Thus the O/C ratios of the first generation SOA products are a good representation of the bulk SOA as measured by the AMS. Kautzman et al. (2009) observed no oligomerization in naphthalene-SOA, hence condensation reactions are likely non-existent which allows the elemental ratios measured by the AMS likely represent the individual species

ACPD
9, 27485–27542, 2009

detected through filter sampling. Artifacts of chromatographic separation may also lead to a bias in the detection of oligomers (Hallquist et al., 2009). Because of the reversibility of condensation reactions, oligomers can hydrolyze, increasing the oxygenation of the species detected. Double-bonds can also hydrate, further increasing the O/C ratio of detected compounds. Further work is needed in characterizing the extent of oligomerization in SOA.

4.3 Uncertainty in the AMS elemental analysis

Uncertainty of the AMS elemental analysis method can contribute to discrepancies in elemental ratios. Uncorrected O/C measurements tend to be biased low due to the propensity of oxygen-containing fragments to be neutral and therefore undetected (Aiken et al., 2007). As a result, the raw measurement of elemental ratios requires calibration factors derived from the analysis of laboratory standards. Many of those standards are large alkanols and alkanoic acids or aromatic species, which are quite similar to the compounds detected in α-pinene and naphthalene-SOA. By contrast, few of the standards have structures similar to the species found in glyoxal, isoprene, and aromatic SOA such as polyols, small organic acids, or larger oligioesters. As more standards become available or as methods to measure hard to sample species are developed, the calibration factors should be revised to reflect ambient OA. It is also possible that the default treatment of O^+, OH^+ and H_2O^+ ions may be inappropriate for glyoxal-SOA. The glyoxal uptake experiments were carried out at relative humidities of at least 60% so as to produce moist ammonium sulfate seed aerosol. The particle-phase water plays an integral role in promoting uptake and oligomerization through hydration, likely leading to larger organic signals at O^+, OH^+ and H_2O^+. The contributions of these ions are based on the $CO_2{}^+$ organic signal, which is very low for glyoxal-SOA, possibly contributing to an underestimate of H/C and O/C ratios.

Underestimates in elemental ratios may also be a result of the exclusion of "NH family" ions and "SO family" ions. These ions were not included as part of the organic mass because most of their signals could be attributed to ammonium sulfate seed aerosol.

Yet, various studies have shown that inorganic constituents of aerosol may react with organics to form new species (Hallquist et al., 2009). For example, Galloway et al. (2009) demonstrated the formation of reduced nitrogen-containing compounds, particularly imidazoles, from a proposed reaction of ammonium and glyoxal. Other studies have observed organosulfates ($R-OSO_3$), organonitrates, and nitrated organosulfates in SOA produced from the photooxidation of isoprene in the presence of ammonium sulfate seed (Surratt et al., 2006, 2007, 2009). Kautzman et al. (2009) observed hydroxybenzene sulfonic in acid in naphthalene SOA in both high and low-NO_x regimes. All of these compounds likely produce NH or SO family ions upon measurement, and their exclusion will negatively bias N/C, H/C, O/C, and S/C values. S/C ratios were considered zero, as no sulfur-containing ions were measured apart from SO family ions.

4.4 AMS marker ions and SOA oxygenation

Analysis of the elemental contributions of different AMS marker ions can provide insight into the possible bulk chemistry occurring in the particle phase. In the oxidative systems studied here (α-pinene, isoprene, single-ring aromatics, and naphthalene), the ions $C_2H_3O^+$ and $CO_2{}^+$ at *m/z* 43 and 44, respectively, contribute strongly to the oxygen content of the formed SOA. In past AMS studies, $C_2H_3O^+$ is prominent in freshly oxidized SOA while $CO_2{}^+$ appears strongly in the spectra of aged OA and laboratory standards of organic acids (Takegawa et al., 2007; Zhang et al., 2005a, 2007; Ulbrich et al., 2009). The spectra presented in the current experiments support these general observations, as the $C_2H_3O^+$ signal is relatively prominent early in the experiments but its fraction of the total organic signal decreases as that of $CO_2{}^+$ increases. In a recent study by Kroll et al. (2009) of heterogeneously oxidized squalane particles, the initial increase of $C_2H_3O^+$ signal was associated with functionalization reactions, those that add oxygen to the carbon chain. With further oxidation, the $CO_2{}^+$ signal increased, which was associated with fragmentation reactions, those associated with C-C bond

scission and subsequent loss of relatively small carbon fragments. It is likely that such processes are , either heterogeneously or in the gas phase, in the systems evaluated here, especially for the single-ring aromatic and naphthalene systems where the O/C ratio continues to increase even as the total particulate volume decreases (Fig. 13 for example). Although time-dependent densities were not measured and wall losses may contribute to the declining particulate volume, it is likely that the continued O/C increase is occurring through fragmentation reactions that are removing carbon from the particle phase. More study is needed to elucidate the contributions of functionalization and fragmentation pathways of SOA.

Recently Aiken et al. (2008) derived a correlation (Eq. 4) between f_{44}, the fraction of organic signal at *m/z* 44 and the O/C measured from the elemental analysis method. Using this correlation, we can evaluate the extent to which f_{44} captures the relative oxygenation of SOA formed in chamber studies. This correlation along with ambient Mexico City data and data from the systems evaluated here are shown in Fig. 15. Supplemental Figs. S1–S7: http://www.atmos-chem-phys-discuss.net/9/27485/2009/acpd-9-27485-2009-supplement.pdf compare O/C_{HR} to O/C_{44} for each system as a function of time. For most oxidant/precursor systems, O/C_{44} mimics the overall trend of O/C_{HR} well. For the α-pinene/O_3, isoprene/high-NO_x, and naphthalene SOA systems, the close correspondence of O/C_{44} and O/C_{HR} results because CO_2^+ provides much of the oxygen signal in the spectra. For the single ring aromatic systems, O/C_{44} is consistently below O/C_{HR} but trends with it. For the isoprene/low-NO_x system, O/C_{44} underestimates O/C_{HR} by 50% early in the oxidation, but then increases to meet O/C_{HR}. For these systems, other mass fragments, especially *m/z* 43 ($C_2H_3O^+$), contribute a large part of the oxygen content. As the contribution of *m/z* 44 grows in these experiments, O/C_{44} becomes a better surrogate for O/C_{HR}. Glyoxal-SOA is a special case because CO_2^+ represents less than 1% of the total organic signal. Although hydrated glyoxal and its oligomers are highly oxygenated, they do not contain acid groups that can easily fragment into CO_2^+. Thus *m/z* 44 is a poor surrogate for estimating the oxygen content of glyoxal SOA. In general, *m/z* 44, adequately

represents the oxygenation of SOA in different oxidative systems, especially for more aged SOA, and for SOA where *m/z* 44 has the largest contribution to the spectral signal. In the ambient atmophere, *m/z* 44 and the correlation determined by Aiken et al. (2008) may better reflect the oxygen content of SOA because ambient SOA represents a very large mixture of compounds from many different VOCs whereas chamber SOA is relatively more homogeneous.

5 Comparison of chamber and ambient elemental ratios and spectra

Figure 16 shows the range of O/C ratios determined from the set of chamber experiments evaluated here, as compared with ambient O/C measurements of Mexico City SOA. Chamber SOA O/C ratios are plotted as a function of precursor carbon number, and the bars represent the maximum range of O/C values observed for each VOC precursor. The dotted lines represent the average O/C values for different sampling times and areas in Mexico City (Aiken et al., 2008), showing that the O/C ratios increase with photochemical age. The shaded regions depict the range of O/C ratios commonly attributed to the different PMF components found for various ambient data sets (Aiken et al., 2008, 2009; Ulbrich et al., 2009; Zhang et al., 2005a,b, 2007), including oxygenated organic aerosol (OOA), biomass burning organic aerosol (BBOA), and hydrocarbon-like organic aerosol (HOA). These ranges and factors are not definite for all ambient data sets but typify the oxygenation domains for commonly derived PMF factors. Often, the OOA is found to consist of two factors: the LV-OOA PMF component is considered to represent aged organic aerosol with a higher O/C ratio than SV-OOA which is considered to represent relatively fresh SOA.

While one might expect SOA O/C ratios to decrease as the carbon number of the precursor system increases, individual differences in elemental composition depend greatly on the identity of the precursor and mechanism, and the duration of oxidation. In the experiments surveyed here, photooxidation of aromatic precursor systems (toluene, *m*-xylene, and naphthalene) produces SOA that achieves higher O/C ratios than the

biogenic systems (isoprene photooxidation and α-pinene ozonolysis). While this is not necessarily representative of ambient SOA formation, it does provide context to compare the SOA O/C ratios measured in ambient atmosphere to those from chamber experiments. Previous studies have noted that AMS mass spectra of chamber data do not exhibit as much oxidation as the OOA mass spectrum, with the possible exception of SOA derived from aromatic precursors (Zhang et al., 2005a; Bahreini et al., 2005). The laboratory data evaluated here show that for photooxidation-SOA, O/C ratios of at least 0.5 are achieved, an oxidation state comparable to that of SV-OOA. Aromatic and naphthalene photooxidation yield SOA that increases in O/C ratios throughout the experiments, regardless of NO_x condition, reaching upwards of 0.7, well into what might be considered as the oxygenation state of LV-OOA. Generally chamber studies do not reach the highest O/C ratios observed in remote OA, which can approach unity (DeCarlo et al., 2008). This emphasizes the need to devise chamber experiments that achieve sufficient timescales to achieve the OH exposure needed to form the most oxygenated SOA (Hallquist et al., 2009).

In addition to elemental composition, comparisons between PMF component spectra and chamber spectra from the AMS can provide insight into the extent to which chamber systems represent ambient SOA. The typical HOA spectrum is identified by its $C_nH_{2n+1}^+$ and $C_nH_{2n-1}^+$ ion series, characteristic of hydrocarbon spectra. On the other hand, the OOA spectrum is distinguished by a strong peak at *m/z* 44 (CO_2^+) and relatively little signal at *m/z*>55. In its subclasses, SV-OOA has a prominent *m/z* 43 ($C_2H_3O^+$) signal, and LV-OOA has a dominant *m/z* 44 signal. Of the systems surveyed here, aromatic (toluene, *m*-xylene, and naphthalene) and isoprene high-NO_x spectra most resemble that of OOA, with prominent contributions at $C_2H_3O^+$ and CO_2^+ and relatively small signals at higher mass-to-charge ratios. Naphthalene spectra best resemble LV-OOA with a dominant *m/z* 44 signal; they do, however, have fairly sizable signals at hydrocarbon-like ions, likely from the fragmentation of a retained aromatic ring. The spectra of *m*-xylene, toluene and isoprene-high-NO_x resemble that of SV-OOA with strong contributions at $C_2H_3O^+$. The steady increase of f_{44} throughout the

duration of single-ring aromatic photooxidation suggests that with continued irradiation the spectra will look more like that of LV-OOA. Consistent with measured O/C ratios, the spectrum of SOA from α-pinene ozonolysis is the least oxidized; along with a prominent $C_2H_3O^+$ contribution, the spectrum shown in Fig. 2b has considerable signals of hydrocarbon-like ions in series similar to that of HOA. One should note that the organic loadings for the α-pinene system were relatively large, and that at smaller loadings the spectrum will be more similar to that of OOA (Shilling et al., 2009). Interestingly, the spectrum of the most oxidized system, glyoxal uptake, least resembles the spectra of previously identified PMF components. The dominant CHO^+ ion and other notable ions that exist in the valleys of typical ions series, such as $CH_3O_2^+$ and $C_2H_2O_2^+$, in the glyoxal-SOA spectrum suggest that if glyoxal uptake is occurring in ambient systems, these ions would be prominent in ambient spectra; they do appear in OOA spectra (Aiken et al., 2009, Sup. Matl.) but not at the percent of the total spectral signal observed here. If reactive uptake of glyoxal occurs substantially in ambient SOA, its contribution to AMS spectra may be obscured by the presence of other species or by its participation in particle-phase reactions.

The work here presents high resolution AMS data of a canonical ensemble of chamber SOA systems. While not representing the most oxidized ambient SOA, the spectra and elemental composition measurements of the surveyed systems could provide a basis for linking chamber data to ambient measurements and understanding ambient PMF factors, especially the SV-OOA component. However, more work is needed to correlate AMS spectra with molecular structure, and experiments need to be devised that can reach the oxidation states achieved in ambient systems to further interpret the the full transformation of VOCs to OOA.

Acknowledgements. This work was supported by the US Department of Energy Biological and Environmental Research grant DE-FG02-05ER63983, US Environmental Protection Agency STAR grant RD-83374901, and US NSF grant ATM-0432377. It has not been formally reviewed by EPA. The views expressed in this document are solely those of the authors and the EPA does not endorse any products in this publication. The authors would like to thank Arthur Chan, Jason Surratt and Nga Lee Ng for helpful discussions and Man Nin Chan for analysis of filter samples.

References

Aiken, A. C., DeCarlo, P. F., and Jimenez, J. L.: Elemental analysis of organic species with electron ionization high-resolution mass spectrometry, Anal. Chem., 79, 8350–8358, doi:10.1021/Ac071150w, 2007. 27487, 27491, 27492, 27508

Aiken, A. C., Decarlo, P. F., Kroll, J. H., Worsnop, D. R., Huffman, J. A., Docherty, K. S., Ulbrich, I. M., Mohr, C., Kimmel, J. R., Sueper, D., Sun, Y., Zhang, Q., Trimborn, A., Northway, M., Ziemann, P. J., Canagaratna, M. R., Onasch, T. B., Alfarra, M. R., Prevot, A. S. H., Dommen, J., Duplissy, J., Metzger, A., Baltensperger, U., and Jimenez, J. L.: O/C and OM/OC ratios of primary, secondary, and ambient organic aerosols with high-resolution time-of-flight aerosol mass spectrometry, Environ. Sci. Technol., 42, 4478–4485, doi:10.1021/Es703009q, 2008. 27487, 27488, 27492, 27493, 27495, 27497, 27510, 27511, 27526, 27541, 27542

Aiken, A. C., Salcedo, D., Cubison, M. J., Huffman, J. A., DeCarlo, P. F., Ulbrich, I. M., Docherty, K. S., Sueper, D., Kimmel, J. R., Worsnop, D. R., Trimborn, A., Northway, M., Stone, E. A., Schauer, J. J., Volkamer, R. M., Fortner, E., de Foy, B., Wang, J., Laskin, A., Shutthanandan, V., Zheng, J., Zhang, R., Gaffney, J., Marley, N. A., Paredes-Miranda, G., Arnott, W. P., Molina, L. T., Sosa, G., and Jimenez, J. L.: Mexico City aerosol analysis during MILAGRO using high resolution aerosol mass spectrometry at the urban supersite (T0) - Part 1: Fine particle composition and organic source apportionment, Atmos. Chem. Phys., 9, 6633–6653, 2009, http://www.atmos-chem-phys.net/9/6633/2009/. 27487, 27511, 27513, 27542

Allan, J. D., Delia, A. E., Coe, H., Bower, K. N., Alfarra, M. R., Jimenez, J. L., Middlebrook, A. M., Drewnick, F., Onasch, T. B., Canagaratna, M. R., Jayne, J. T., and

Worsnopf, D. R.: A generalised method for the extraction of chemically resolved mass spectra from aerodyne aerosol mass spectrometer data, J. Aerosol Sci., 35, 909–922, doi:10.1016/j.jaerosci.2004.02.007, 2004. 27491

Alvarez, E. G., Viidanoja, J., Munoz, A., Wirtz, K., and Hjorth, J.: Experimental confirmation of the dicarbonyl route in the photo-oxidation of toluene and benzene, Environ. Sci. Technol., 41, 8362–8369, doi:10.1021/Es0713274, 2007. 27505

Atkinson, R., Aschmann, S. M., Arey, J., Zielinska, B., and Schuetzle, D.: Gas-phase atmospheric chemistry of 1-Nitronaphthalene and 2-Nitronaphthalene and 1,4-Naphthoquinone, Atmos. Environ., 23, 2679–2690, 1989. 27504

Bahreini, R., Keywood, M. D., Ng, N. L., Varutbangkul, V., Gao, S., Flagan, R. C., Seinfeld, J. H., Worsnop, D. R., and Jimenez, J. L.: Measurements of secondary organic aerosol from oxidation of cycloalkenes, terpenes, and *m*-xylene using an Aerodyne aerosol mass spectrometer, Environ. Sci. Technol., 39, 5674–5688, doi:10.1021/Es048061a, 2005. 27489, 27512, 27524

Bloss, C., Wagner, V., Jenkin, M. E., Volkamer, R., Bloss, W. J., Lee, J. D., Heard, D. E., Wirtz, K., Martin-Reviejo, M., Rea, G., Wenger, J. C., and Pilling, M. J.: Development of a detailed chemical mechanism (MCMv3.1) for the atmospheric oxidation of aromatic hydrocarbons, Atmos. Chem. Phys., 5, 641–664, 2005, http://www.atmos-chem-phys.net/5/641/2005/. 27502, 27505

Canagaratna, M. R., Jayne, J. T., Jimenez, J. L., Allan, J. D., Alfarra, M. R., Zhang, Q., Onasch, T. B., Drewnick, F., Coe, H., Middlebrook, A., Delia, A., Williams, L. R., Trimborn, A. M., Northway, M. J., DeCarlo, P. F., Kolb, C. E., Davidovits, P., and Worsnop, D. R.: Chemical and microphysical characterization of ambient aerosols with the aerodyne aerosol mass spectrometer, Mass Spectrom. Rev., 26, 185–222, doi:10.1002/Mas.20115, 2007. 27486, 27491

Chan, A. W. H., Kautzman, K. E., Chhabra, P. S., Surratt, J. D., Chan, M. N., Crounse, J. D., Kürten, A., Wennberg, P. O., Flagan, R. C., and Seinfeld, J. H.: Secondary organic aerosol formation from photooxidation of naphthalene and alkylnaphthalenes: implications for oxidation of intermediate volatility organic compounds (IVOCs), Atmos. Chem. Phys., 9, 3049–3060, 2009a, http://www.atmos-chem-phys.net/9/3049/2009/. 27488, 27491, 27524

Chan, M. N., Chan, A. W. H., Chhabra, P. S., Surratt, J. D., and Seinfeld, J. H.: Modeling of secondary organic aerosol yields from laboratory chamber data, Atmos. Chem. Phys., 9,

5669–5680, 2009b, http://www.atmos-chem-phys.net/9/5669/2009/. 27488, 27490, 27497
Claeys, M., Graham, B., Vas, G., Wang, W., Vermeylen, R., Pashynska, V., Cafmeyer, J., Guyon, P., Andreae, M. O., Artaxo, P., and Maenhaut, W.: Formation of secondary organic aerosols through photooxidation of isoprene, Science, 303, 1173–1176, 2004. 27498
Cocker, D. R., Flagan, R. C., and Seinfeld, J. H.: State-of-the-art chamber facility for studying atmospheric aerosol chemistry, Environ. Sci. Technol., 35, 2594–2601, doi:10.1021/Es0019169, 2001. 27490
Crable, G. F. and Coggeshall, N. D.: Application of total ionization principles to mass spectrometric analysis, Anal. Chem., 30, 310–313, 1958. 27491
DeCarlo, P. F., Kimmel, J. R., Trimborn, A., Northway, M. J., Jayne, J. T., Aiken, A. C., Gonin, M., Fuhrer, K., Horvath, T., Docherty, K. S., Worsnop, D. R., and Jimenez, J. L.: Field-deployable, high-resolution, time-of-flight aerosol mass spectrometer, Anal. Chem., 78, 8281–8289, doi:10.1021/Ac061249n, 2006. 27487, 27491
DeCarlo, P. F., Dunlea, E. J., Kimmel, J. R., Aiken, A. C., Sueper, D., Crounse, J., Wennberg, P. O., Emmons, L., Shinozuka, Y., Clarke, A., Zhou, J., Tomlinson, J., Collins, D. R., Knapp, D., Weinheimer, A. J., Montzka, D. D., Campos, T., and Jimenez, J. L.: Fast airborne aerosol size and chemistry measurements above Mexico City and Central Mexico during the MILAGRO campaign, Atmos. Chem. Phys., 8, 4027–4048, 2008, http://www.atmos-chem-phys.net/8/4027/2008/. 27487, 27512
Dommen, J., Metzger, A., Duplissy, J., Kalberer, M., Alfarra, M. R., Gascho, A., Weingartner, E., Prevot, A. S. H., Verheggen, B., and Baltensperger, U.: Laboratory observation of oligomers in the aerosol from isoprene/NO_x photooxidation, Geophys. Res. Lett., 33, L13805, doi:10.1029/2006gl026523, 2006. 27507
Drewnick, F., Hings, S. S., DeCarlo, P., Jayne, J. T., Gonin, M., Fuhrer, K., Weimer, S., Jimenez, J. L., Demerjian, K. L., Borrmann, S., and Worsnop, D. R.: A new time-of-flight aerosol mass spectrometer (TOF-AMS) – instrument description and first field deployment, Aerosol Sci. Tech., 39, 637–658, doi:10.1080/02786820500182040, 2005. 27487
Dzepina, K., Volkamer, R. M., Madronich, S., Tulet, P., Ulbrich, I. M., Zhang, Q., Cappa, C. D., Ziemann, P. J., and Jimenez, J. L.: Evaluation of recently-proposed secondary organic aerosol models for a case study in Mexico City, Atmos. Chem. Phys., 9, 5681–5709, 2009, http://www.atmos-chem-phys.net/9/5681/2009/. 27494
Fisseha, R., Dommen, J., Sax, M., Paulsen, D., Kalberer, M., Maurer, R., Hofler, F.,

Weingartner, E., and Baltensperger, U.: Identification of organic acids in secondary organic aerosol and the corresponding gas phase from chamber experiments, Anal. Chem., 76, 6535–6540, doi:10.1021/Ac048975f, 2004. 27502, 27507

Fratzke, A. R. and Reilly, P. J.: Thermodynamic and kinetic-analysis of the dimerization of aqueous glyoxal, Int. J. Chem. Kinet., 18, 775–789, 1986. 27495

Galloway, M. M., Chhabra, P. S., Chan, A. W. H., Surratt, J. D., Flagan, R. C., Seinfeld, J. H., and Keutsch, F. N.: Glyoxal uptake on ammonium sulphate seed aerosol: reaction products and reversibility of uptake under dark and irradiated conditions, Atmos. Chem. Phys., 9, 3331–3345, 2009, http://www.atmos-chem-phys.net/9/3331/2009/. 27488, 27490, 27496, 27509, 27524

Gao, S., Keywood, M., Ng, N. L., Surratt, J., Varutbangkul, V., Bahreini, R., Flagan, R. C., and Seinfeld, J. H.: Low-molecular-weight and oligomeric components in secondary organic aerosol from the ozonolysis of cycloalkenes and alpha-pinene, J. Phys. Chem. A, 108, 10147–10164, doi:10.1021/Jp047466e, 2004. 27497, 27507

Glasius, M., Lahaniati, M., Calogirou, A., Di Bella, D., Jensen, N. R., Hjorth, J., Kotzias, D., and Larsen, B. R.: Carboxylic acids in secondary aerosols from oxidation of cyclic monoterpenes by ozone, Environ. Sci. Technol., 34, 1001–1010, 2000. 27497

Gómez-González, Y., Surratt, J. D., Cuyckens, F., Szmigielski, R., Vermeylen, R., Jaoui, M., Lewandowski, M., Offenberg, J. H., Kleindienst, T. E., Edney, E. O., Blockhuys, F., Van Alsenoy, C., Maenhaut, W., and Claeys, M.: Characterization of organosulfates from the photooxidation of isoprene and unsaturated fatty acids in ambient aerosol using liquid chromatography/(-) electrospray ionization mass spectrometry, J. Mass Spectrom., 43, 371–382, doi:10.1002/Jms.1329, 2008. 27499

Hallquist, M., Wenger, J. C., Baltensperger, U., Rudich, Y., Simpson, D., Claeys, M., Dommen, J., Donahue, N. M., George, C., Goldstein, A. H., Hamilton, J. F., Herrmann, H., Hoffmann, T., Iinuma, Y., Jang, M., Jenkin, M. E., Jimenez, J. L., Kiendler-Scharr, A., Maenhaut, W., McFiggans, G., Mentel, T. F., Monod, A., Prévôt, A. S. H., Seinfeld, J. H., Surratt, J. D., Szmigielski, R., and Wildt, J.: The formation, properties and impact of secondary organic aerosol: current and emerging issues, Atmos. Chem. Phys., 9, 5155–5235, 2009, http://www.atmos-chem-phys.net/9/5155/2009/. 27486, 27508, 27509, 27512

Hamilton, J. F., Lewis, A. C., Bloss, C., Wagner, V., Henderson, A. P., Golding, B. T., Wirtz, K., Martin-Reviejo, M., and Pilling, M. J.: Measurements of photo-oxidation products from the reaction of a series of alkyl-benzenes with hydroxyl radicals during EXACT using

comprehensive gas chromatography, Atmos. Chem. Phys., 3, 1999–2014, 2003, http://www.atmos-chem-phys.net/3/1999/2003/. 27502

Hamilton, J. F., Webb, P. J., Lewis, A. C., and Reviejo, M. M.: Quantifying small molecules in secondary organic aerosol formed during the photo-oxidation of toluene with hydroxyl radicals, Atmos. Environ., 39, 7263–7275, doi:10.1016/j.atmosenv.2005.09.006, 2005. 27502, 27503

Heaton, K. J., Dreyfus, M. A., Wang, S., and Johnston, M. V.: Oligomers in the early stage of biogenic secondary organic aerosol formation and growth, Environ. Sci. Technol., 41, 6129–6136, doi:10.1021/Es070314n, 2007. 27526

Huffman, J. A., Docherty, K. S., Mohr, C., Cubison, M. J., Ulbrich, I. M., Ziemann, P. J., Onasch, T. B., and Jimenez, J. L.: Chemically-resolved volatility measurements of organic aerosol from different sources, Environ. Sci. Technol., 43, 5351–5357, doi:10.1021/Es803539d, 2009. 27488

Iinuma, Y., Boge, O., Gnauk, T., and Herrmann, H.: Aerosol-chamber study of the alpha-pinene/O-3 reaction: influence of particle acidity on aerosol yields and products, Atmos. Environ., 38, 761–773, doi:10.1016/j.atmosenv.2003.10.015, 2004. 27497

Ip, H. S. S., Huang, X. H. H., and Yu, J. Z.: Effective Henry's law constants of glyoxal, glyoxylic acid, and glycolic acid, Geophys. Res. Lett., 36, L01802, doi:10.1029/2008gl036212, 2009. 27504

Jang, M. and Kamens, R. M.: Newly characterized products and composition of secondary aerosols from the reaction of alpha-pinene with ozone, Atmos. Environ., 33, 459–474, 1999. 27497

Jang, M. S. and Kamens, R. M.: Characterization of secondary aerosol from the photooxidation of toluene in the presence of NO_x and 1-propene, Environ. Sci. Technol., 35, 3626–3639, doi:10.1021/Es010676+, 2001. 27502, 27503

Jayne, J. T., Leard, D. C., Zhang, X. F., Davidovits, P., Smith, K. A., Kolb, C. E., and Worsnop, D. R.: Development of an aerosol mass spectrometer for size and composition analysis of submicron particles, Aerosol Sci. Tech., 33, 49–70, 2000. 27486

Jimenez, J. L., Jayne, J. T., Shi, Q., Kolb, C. E., Worsnop, D. R., Yourshaw, I., Seinfeld, J. H., Flagan, R. C., Zhang, X. F., Smith, K. A., Morris, J. W., and Davidovits, P.: Ambient aerosol sampling using the Aerodyne Aerosol Mass Spectrometer, J. Geophys. Res.-Atmos., 108(D7), 8425, doi:10.1029/2001jd001213, 2003. 27486, 27491

Jimenez, J. L., Canagaratna, M. R., Donahue, N. M., Prevot, A. S. H., Zhang, Q., Kroll, J. H.,

DeCarlo, P. F., Allan, J. D., Coe, H., Ng, N. L., Aiken, A. C., Docherty, K. D., Ulbrich, I. M., Grieshop, A. P., Robinson, A. L., Duplissy, J., Smith, J. D., Wilson, K. R., Lanz, V. A., Hueglin, C., Sun, Y. L., Tian, J., Laaksonen, A., Raatikainen, T., Rautiainen, J., Vaattovaara, P., Ehn, M., Kulmala, M., Tomlinson, J. M., Collins, D. R., Cubison, M. J., Dunlea, E. J., Huffman, J. A., Onasch, T. B., Alfarra, M. R., Williams, P. I., Bower, K., Kondo, Y., Schneider, J., Drewnick, F., Borrmann, S., Weimer, S., Demerjian, K., Salcedo, D., Cottrell, L., Griffin, R., Takami, A., Miyoshi, T., Hatakeyama, S., Shimono, A., Sun, J. Y., Zhang, Y. M., Dzepina, K., Kimmel, J. R., Sueper, D., Jayne, J. T., Herndon, S. C., Trimborn, A. M., Williams, L. R., Wood, E. C., Kolb, C. E., Middlebrook, A. M., Baltensperger, U., and Worsnop, D. R.: Evolution of organic aerosols in the atmosphere, Science, 326(5959), 1525–1529, doi:10.1126/science.1180353, 2009. 27489

Kalberer, M., Paulsen, D., Sax, M., Steinbacher, M., Dommen, J., Prevot, A. S. H., Fisseha, R., Weingartner, E., Frankevich, V., Zenobi, R., and Baltensperger, U.: Identification of polymers as major components of atmospheric organic aerosols, Science, 303, 1659–1662, 2004. 27502, 27507

Kautzman, K. E., Surratt, J. D., Chan, M. N., Chan, A. W. H., Hersey, S. P., Chhabra, P. S., Dalleska, N. F., Wennberg, P. O., Flagan, R. C., and Seinfeld, J. H.: Chemical composition of gas- and aerosol-phase products from the photooxidation of naphthalene, J. Phys. Chem. A, doi:1021/jp908530s, 2009. 27488, 27503, 27504, 27505, 27506, 27507, 27509

Keywood, M. D., Kroll, J. H., Varutbangkul, V., Bahreini, R., Flagan, R. C., and Seinfeld, J. H.: Secondary organic aerosol formation from cyclohexene ozonolysis: effect of OH scavenger and the role of radical chemistry, Environ. Sci. Technol., 38, 3343–3350, doi:10.1021/Es049725j, 2004. 27490

Koch, S., Winterhalter, R., Uherek, E., Kolloff, A., Neeb, P., and Moortgat, G. K.: Formation of new particles in the gas-phase ozonolysis of monoterpenes, Atmos. Environ., 34, 4031–4042, 2000. 27497

Kroll, J. H. and Seinfeld, J. H.: Chemistry of secondary organic aerosol: Formation and evolution of low-volatility organics in the atmosphere, Atmos. Environ., 42, 3593–3624, doi:10.1016/j.atmosenv.2008.01.003, 2008. 27486, 27489

Kroll, J. H., Ng, N. L., Murphy, S. M., Flagan, R. C., and Seinfeld, J. H.: Secondary organic aerosol formation from isoprene photooxidation, Environ. Sci. Technol., 40, 1869–1877, doi:10.1021/Es0524301, 2006. 27491, 27498, 27524

Kroll, J. H., Smith, J. D., Che, D. L., Kessler, S. H., Worsnop, D. R., and Wilson, K. R.:

Measurement of fragmentation and functionalization pathways in the heterogeneous oxidation of oxidized organic aerosol, Phys. Chem. Chem. Phys., 11, 8005–8014, doi:10.1039/B905289e, 2009. 27488, 27509

Kua, J., Hanley, S. W., and De Haan, D. O.: Thermodynamics and kinetics of glyoxal dimer formation: a computational study, J. Phys. Chem. A, 112, 66–72, doi:10.1021/Jp076573g, 2008. 27495

Lanz, V. A., Alfarra, M. R., Baltensperger, U., Buchmann, B., Hueglin, C., and Prévôt, A. S. H.: Source apportionment of submicron organic aerosols at an urban site by factor analytical modelling of aerosol mass spectra, Atmos. Chem. Phys., 7, 1503–1522, 2007, http://www.atmos-chem-phys.net/7/1503/2007/. 27489

Lee, M. H., Heikes, B. G., and O'Sullivan, D. W.: Hydrogen peroxide and organic hydroperoxide in the troposphere: a review, Atmos. Environ., 34, 3475–3494, 2000. 27499

Loeffler, K. W., Koehler, C. A., Paul, N. M., and De Haan, D. O.: Oligomer formation in evaporating aqueous glyoxal and methyl glyoxal solutions, Environ. Sci. Technol., 40, 6318–6323, doi:10.1021/Es060810w, 2006. 27495, 27504

Malloy, Q. G. J., Li Qi, , Warren, B., Cocker III, D. R., Erupe, M. E., and Silva, P. J.: Secondary organic aerosol formation from primary aliphatic amines with NO_3 radical, Atmos. Chem. Phys., 9, 2051–2060, 2009, http://www.atmos-chem-phys.net/9/2051/2009/. 27488

Mohr, C., Huffman, J. A., Cubison, M. J., Aiken, A. C., Docherty, K. S., Kimmel, J. R., Ulbricht, I. M., Hannigan, M., and Jimenez, J. L.: Characterization of primary organic aerosol emissions from meat cooking, trash burning, and motor vehicles with high-resolution aerosol mass spectrometry and comparison with ambient and chamber observations, Environ. Sci. Technol., 43, 2443–2449, doi:10.1021/Es8011518, 2009. 27488

Ng, N. L., Kroll, J. H., Keywood, M. D., Bahreini, R., Varutbangkul, V., Flagan, R. C., Seinfeld, J. H., Lee, A., and Goldstein, A. H.: Contribution of first- versus second-generation products to secondary organic aerosols formed in the oxidation of biogenic hydrocarbons, Environ. Sci. Technol., 40, 2283–2297, doi:10.1021/Es052269u, 2006. 27505

Ng, N. L., Kroll, J. H., Chan, A. W. H., Chhabra, P. S., Flagan, R. C., and Seinfeld, J. H.: Secondary organic aerosol formation from m-xylene, toluene, and benzene, Atmos. Chem. Phys., 7, 3909–3922, 2007, http://www.atmos-chem-phys.net/7/3909/2007/. 7. 27491, 27524

Reinhardt, A., Emmenegger, C., Gerrits, B., Panse, C., Dommen, J., Baltensperger, U.,

Zenobi, R., and Kalberer, M.: Ultrahigh mass resolution and accurate mass measurements as a tool to characterize oligomers in secondary organic aerosols, Anal. Chem., 79, 4074–4082, doi:10.1021/Ac062425v, 2007. 27497, 27526

Renbaum, L. H. and Smith, G. D.: Organic nitrate formation in the radical-initiated oxidation of model aerosol particles in the presence of NO_x, Phys. Chem. Chem. Phys., 11, 8040–8047, doi:10.1039/B909239k, 2009. 27501

Roberts, J. M. and Fajer, R. W.: Uv absorption cross-sections of organic nitrates of potential atmospheric importance and estimation of atmospheric lifetimes, Environ. Sci. Technol., 23, 945–951, 1989. 27501

Sato, K.: Detection of nitrooxypolyols in secondary organic aerosol formed from the photooxidation of conjugated dienes under high-NO_x conditions, Atmos. Environ., 42, 6851–6861, doi:10.1016/j.atmosenv.2008.05.010, 2008. 27501

Sato, K., Hatakeyama, S., and Imamura, T.: Secondary organic aerosol formation during the photooxidation of toluene: NO_x dependence of chemical composition, J. Phys. Chem. A, 111, 9796–9808, doi:10.1021/Jp071419f, 2007. 27502, 27503

Shilling, J. E., Chen, Q., King, S. M., Rosenoern, T., Kroll, J. H., Worsnop, D. R., DeCarlo, P. F., Aiken, A. C., Sueper, D., Jimenez, J. L., and Martin, S. T.: Loading-dependent elemental composition of a-pinene SOA particles, Atmos. Chem. Phys., 9, 771–782, 2009, http://www.atmos-chem-phys.net/9/771/2009/. 27488, 27497, 27498, 27513, 27526

Smith, J. D., Kroll, J. H., Cappa, C. D., Che, D. L., Liu, C. L., Ahmed, M., Leone, S. R., Worsnop, D. R., and Wilson, K. R.: The heterogeneous reaction of hydroxyl radicals with sub-micron squalane particles: a model system for understanding the oxidative aging of ambient aerosols, Atmos. Chem. Phys., 9, 3209–3222, 2009, http://www.atmos-chem-phys.net/9/3209/2009/. 27488

Sun, Y., Zhang, Q., Macdonald, A. M., Hayden, K., Li, S. M., Liggio, J., Liu, P. S. K., Anlauf, K. G., Leaitch, W. R., Steffen, A., Cubison, M., Worsnop, D. R., van Donkelaar, A., and Martin, R. V.: Size-resolved aerosol chemistry on Whistler Mountain, Canada with a high-resolution aerosol mass spectrometer during INTEX-B, Atmos. Chem. Phys., 9, 3095–3111, 2009, http://www.atmos-chem-phys.net/9/3095/2009/. 27488

Surratt, J. D., Murphy, S. M., Kroll, J. H., Ng, N. L., Hildebrandt, L., Sorooshian, A., Szmigielski, R., Vermeylen, R., Maenhaut, W., Claeys, M., Flagan, R. C., and Seinfeld, J. H.: Chemical composition of secondary organic aerosol formed from the photooxidation of isoprene, J. Phys. Chem. A, 110, 9665–9690, doi:10.1021/Jp061734m, 2006. 27499, 27500, 27506,

27507, 27509
Surratt, J. D., Lewandowski, M., Offenberg, J. H., Jaoui, M., Kleindienst, T. E., Edney, E. O., and Seinfeld, J. H.: Effect of acidity on secondary organic aerosol formation from isoprene, Environ. Sci. Technol., 41, 5363–5369, doi:10.1021/Es0704176, 2007. 27499, 27507, 27509
Surratt, J. D., Gómez-Gónzalez, Y., Chan, A. W. H., Vermeylen, R., Shahgholi, M., Kleindienst, T. E., Edney, E. O., Offenberg, J. H., Lewandowski, M., Jaoui, M., Maenhaut, W., Claeys, M., Flagan, R. C., and Seinfeld, J. H.: Organosulfate formation in biogenic secondary organic aerosol, J. Phys. Chem. A, 112, 8345–8378, doi:10.1021/jp802310p, 2008. 27499
Surratt, J. D., Chan, A. W. H., Eddingsaas, N. C., Chan, M. N., Loza, C. L., Kwan, A. J., Hersey, S. P., Flagan, R. C., Wennberg, P. O., and Seinfeld, J. H.: Reactive intermediates revealed in secondary organic aerosol formation from isoprene, Proc. Natl. Acad. Sci. USA, in press, 2009. 27499, 27500, 27501, 27506, 27507, 27509
Szmigielski, R., Surratt, J. D., Vermeylen, R., Szmigielska, K., Kroll, J. H., Ng, N. L., Murphy, S. M., Sorooshian, A., Seinfeld, J. H., and Claeys, M.: Characterization of 2-methylglyceric acid oligomers in secondary organic aerosol formed from the photooxidation of isoprene using trimethylsilylation and gas chromatography/ion trap mass spectrometry, J. Mass Spectrom., 42, 101–116, doi:10.1002/Jms.1146, 2007. 27500, 27506, 27507
Takegawa, N., Miyakawa, T., Kawamura, K., and Kondo, Y.: Contribution of selected dicarboxylic and omega-oxocarboxylic acids in ambient aerosol to the *m/z* 44 signal of an aerodyne aerosol mass spectrometer, Aerosol Sci. Tech., 41, 418–437, doi:10.1080/02786820701203215, 2007. 27492, 27509
Tolocka, M. P., Heaton, K. J., Dreyfus, M. A., Wang, S. Y., Zordan, C. A., Saul, T. D., and Johnston, M. V.: Chemistry of particle inception and growth during α-pinene ozonolysis, Environ. Sci. Technol., 40, 1843–1848, doi:10.1021/Es051926f, 2006. 27497, 27526
Ulbrich, I. M., Canagaratna, M. R., Zhang, Q., Worsnop, D. R., and Jimenez, J. L.: Interpretation of organic components from Positive Matrix Factorization of aerosol mass spectrometric data, Atmos. Chem. Phys., 9, 2891–2918, 2009, http://www.atmos-chem-phys.net/9/2891/2009/. 27489, 27509, 27511, 27542
Volkamer, R., Martini, F. S., Molina, L. T., Salcedo, D., Jimenez, J. L., and Molina, M. J.: A missing sink for gas-phase glyoxal in Mexico City: formation of secondary organic aerosol, Geophys. Res. Lett., 34, L13805, doi:10.1029/2007gl030752, 2007. 27494
Volkamer, R., Ziemann, P. J., and Molina, M. J.: Secondary Organic Aerosol Formation from

Acetylene (C_2H_2): seed effect on SOA yields due to organic photochemistry in the aerosol aqueous phase, Atmos. Chem. Phys., 9, 1907–1928, 2009, http://www.atmos-chem-phys.net/9/1907/2009/. 27494

Walser, M. L., Desyaterik, Y., Laskin, J., Laskin, A., and Nizkorodov, S. A.: High-resolution mass spectrometric analysis of secondary organic aerosol produced by ozonation of limonene, Phys. Chem. Chem. Phys., 10, 1009–1022, doi:10.1039/B712620d, 2008. 27526

Wang, W., Kourtchev, I., Graham, B., Cafmeyer, J., Maenhaut, W., and Claeys, M.: Characterization of oxygenated derivatives of isoprene related to 2-methyltetrols in Amazonian aerosols using trimethylsilylation and gas chromatography/ion trap mass spectrometry, Rapid Commun. Mass Sp., 19, 1343–1351, doi:10.1002/Rcm.1940, 2005. 27499

Whipple, E. B.: Structure of glyoxal in water, J. Am. Chem. Soc., 92, 7183, doi:10.1021/ja00727a027, 1970. 27495

Yu, J. Z., Cocker, D. R., Griffin, R. J., Flagan, R. C., and Seinfeld, J. H.: Gas-phase ozone oxidation of monoterpenes: gaseous and particulate products, J. Atmos. Chem., 34, 207–258, 1999. 27497, 27505, 27506

Zhang, Q., Alfarra, M. R., Worsnop, D. R., Allan, J. D., Coe, H., Canagaratna, M. R., and Jimenez, J. L.: Deconvolution and quantification of hydrocarbon-like and oxygenated organic aerosols based on aerosol mass spectrometry, Environ. Sci. Technol., 39, 4938–4952, doi:10.1021/Es048568l, 2005a. 27489, 27509, 27511, 27512

Zhang, Q., Worsnop, D. R., Canagaratna, M. R., and Jimenez, J. L.: Hydrocarbon-like and oxygenated organic aerosols in Pittsburgh: insights into sources and processes of organic aerosols, Atmos. Chem. Phys., 5, 3289–3311, 2005b, http://www.atmos-chem-phys.net/5/3289/2005/. 27489, 27511, 27542

Zhang, Q., Jimenez, J. L., Canagaratna, M. R., Allan, J. D., Coe, H., Ulbrich, I., Alfarra, M. R., Takami, A., Middlebrook, A. M., Sun, Y. L., Dzepina, K., Dunlea, E., Docherty, K., DeCarlo, P. F., Salcedo, D., Onasch, T., Jayne, J. T., Miyoshi, T., Shimono, A., Hatakeyama, S., Takegawa, N., Kondo, Y., Schneider, J., Drewnick, F., Borrmann, S., Weimer, S., Demerjian, K., Williams, P., Bower, K., Bahreini, R., Cottrell, L., Griffin, R. J., Rautiainen, J., Sun, J. Y., Zhang, Y. M., and Worsnop, D. R.: Ubiquity and dominance of oxygenated species in organic aerosols in anthropogenically-influenced Northern Hemisphere midlatitudes, Geophys. Res. Lett., 34, L13801, doi:10.1029/2007gl029979, 2007. 27489, 27509, 27511

Table 1. Experimental conditions and results.

Expt.#	VOC System	Experiment Type	RH (%)	$[NO]_0$ (ppb)	$[NO_2]_0$ (ppb)	VOC Reacted (ppb)	Seed Vol. ($\mu m^3\ cm^{-3}$)	ΔM_0(Max)[d] ($\mu g\ m^{-3}$)
1	glyoxal uptake	humid	67	<det[a]	<5	131[b]	84	31.80
2	glyoxal uptake	humid	60	<det[a]	<det[a]	182[b]	87	68.30
3	glyoxal uptake	humid	70	<det[a]	<det[a]	NA	NA	NA
4	α-pinene+O_3	no H_2O_2, dry	5.4	<det[a]	<det[a]	50[c]	12.45	56.84
5	α-pinene+O_3	no H_2O_2, humid	66	<det[a]	<det[a]	50[c]	20.00	83.30
6	α-pinene+O_3	H_2O_2, dry	7.2	<det[a]	<det[a]	50[c]	11.59	121.00
7	α-pinene+O_3	H_2O_2, humid	72.3	<det[a]	<det[a]	50[c]	27.38	183.22
8	isoprene+OH	low NO_x	5.2	<det[a]	<det[a]	49	16.23	3.71
9	isoprene+OH	low NO_x	5.3	<det[a]	<det[a]	49	NA	7.00
10	isoprene+OH	low NO_x	<10	<det[a]	<det[a]	91	10.54	10.47
11	isoprene+OH	high NO_x	<10	518	374	81	11.00	1.35
12	isoprene+OH	high NO_x	<10	536	400	267	11.73	4.27
13	isoprene+OH	high NO_x	<10	591	434	286	13.80	11.83
14	toluene+OH	low NO_x	<10	<det[a]	<det[a]	112	10.86	141.45
15	toluene+OH	high NO_x	<10	583	423	136	9.32	50.26
16	*m*-xylene+OH	low NO_x	<10	<det[a]	<det[a]	114	9.78	190.40
17	*m*-xylene+OH	high NO_x	<10	501	538	200	9.34	52.04
18	naphthalene+OH	low NO_x	7.8	<det[a]	<det[a]	5[c]	10.64	12.15
19	naphthalene+OH	low NO_x	13.9	<det[a]	<det[a]	12	24.52	44.91
20	naphthalene+OH	low NO_x, nucleation	8.1	<det[a]	<det[a]	15[c]	0.00	47.17
21	naphthalene+OH	low NO_x	8.3	<det[a]	<det[a]	20[c]	10.48	53.12
22	naphthalene+OH	low NO_x	9.9	<det[a]	<det[a]	63	12.98	201.75
23	naphthalene+OH	high NO_x	7.7	415	272	5[c]	12.25	5.90
24	naphthalene+OH	high NO_x	6.3	431	370	25[c]	12.82	39.02
25	naphthalene+OH	high NO_x, nucleation	<10	422	222	350[c]	0.00	39.26
26	naphthalene+OH	high NO_x	5.9	401	166	40	14.67	75.43

[a] Below the detection limit of the measurement
[b] Equilibrium concentration
[c] Approximate initial concentration
[d] Mass loadings are calculated by multiplying the change in DMA volume by an estimated density. Estimated densities of glyoxal, α-pinene, isoprene, single-ringed aromatics, and naphthalene SOA were taken from Galloway et al. (2009); Bahreini et al. (2005); Kroll et al. (2006); Ng et al. (2007); Chan et al. (2009a), respectively.

ACPD
9, 27485–27542, 2009

Table 2. Elemental composition of each SOA system. Values represent the average ratio for each experiment at the time of maximum O/C.

VOC System		O/C (max)	H/C	N/C	OM/OC
glyoxal uptake		1.13	1.54	0.01	2.68
α-pinene+O_3		0.43	1.47	0.00	1.70
isoprene+OH		0.61	1.55	0.02	1.96
	low NO_x	0.59	1.64	0.00	1.92
	high NO_x	0.62	1.46	0.04	2.00
aromatics+OH		0.68	1.44	0.04	2.07
	m-xylene, high NO_x	0.66	1.48	0.08	2.09
	m-xylene, low NO_x	0.60	1.54	0.00	1.93
	toluene, high NO_x	0.72	1.38	0.07	2.15
	toluene, low NO_x	0.74	1.39	0.00	2.10
naphthalene+OH		0.62	0.89	0.02	1.93
	low NO_x	0.66	0.88	0.00	1.96
	high NO_x	0.57	0.90	0.04	1.89

Table 3. O/C ratios of various laboratory SOA systems.

System	O/C Ratio	Method	Reference
glyoxal uptake	1.13	HR-ToF-AMS	**This Study**
α-pinene+O_3	0.30–0.43	HR-ToF-AMS	**This Study**
	0.38–0.45	HR-ToF-AMS	Shilling et al. (2009)
	0.27	HR-ToF-AMS	Aiken et al. (2008)
	0.4–0.6	ESI-FTICR-MS	Reinhardt et al. (2007)
	0.37–0.4	NAMS	Tolocka et al. (2006)
β-pinene+O_3	0.45	NAMS	Heaton et al. (2007)
Δ^3-carene+O_3	0.43	NAMS	Heaton et al. (2007)
limonene+O_3	0.45	NAMS	Heaton et al. (2007)
	0.43–0.50	ESI-MS (Orbitrap)	Walser et al. (2008)
sabinene+O_3	0.37	NAMS	Heaton et al. (2007)
α-pinene+NO_x	0.39	HR-ToF-AMS	Aiken et al. (2008)
isoprene+OH	0.41	HR-ToF-AMS	Aiken et al. (2008)
	0.50–0.62	HR-ToF-AMS	**This Study**
toluene+OH	0.43	HR-ToF-AMS	Aiken et al. (2008)
	0.50–0.74	HR-ToF-AMS	This Study
m-xylene+OH	0.50–0.66	HR-ToF-AMS	**This Study**
naphthalene+OH	0.30–0.74	HR-ToF-AMS	**This Study**

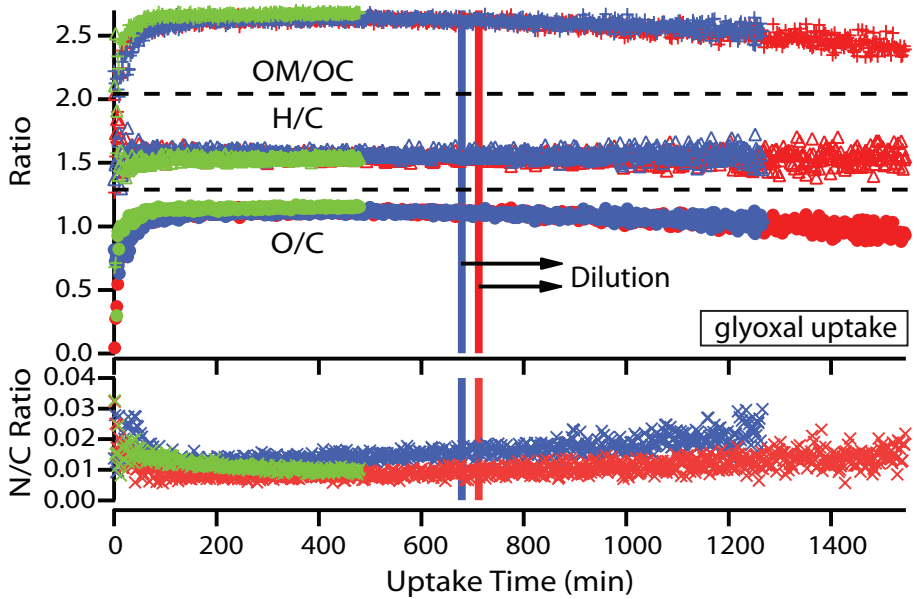

Fig. 1. Experimental profile of elemental ratios and OM/OC for glyoxal uptake experiments. Experiment 1 is in blue, 2 in red and 3 in green. Dotted lines are provided to visually separate different ratios.

ACPD
9, 27485–27542, 2009

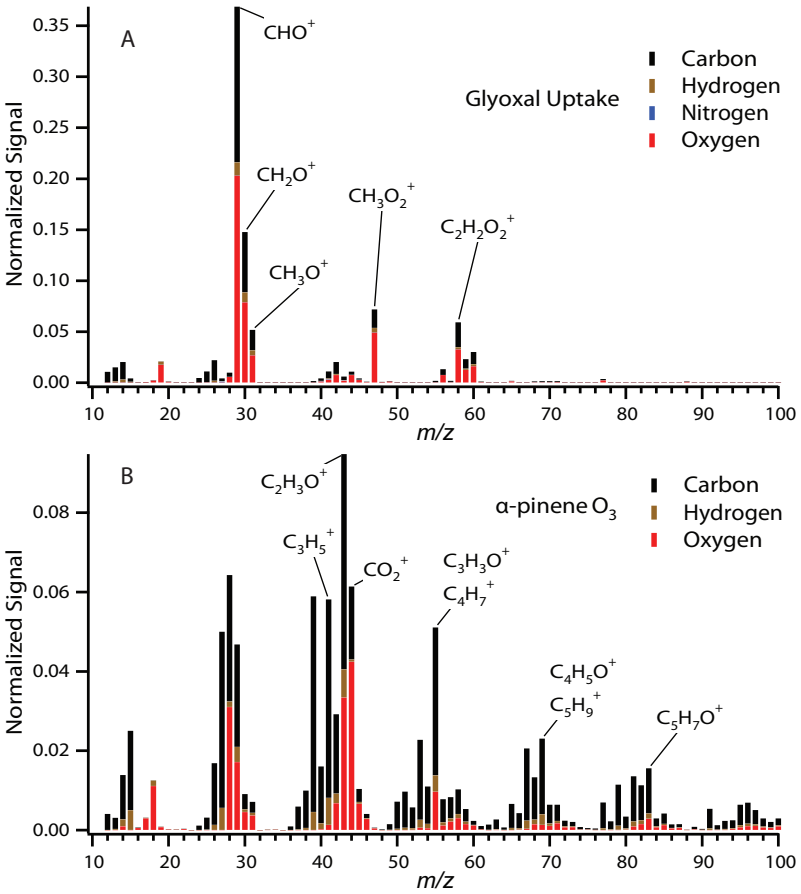

Fig. 2. High-resolution mass spectra of glyoxal **(A)** and α-pinene **(B)** SOA with elemental contributions to each mass-to-charge ratio shown. Spectra are taken at the peak of SOA growth.

ACPD
9, 27485–27542, 2009

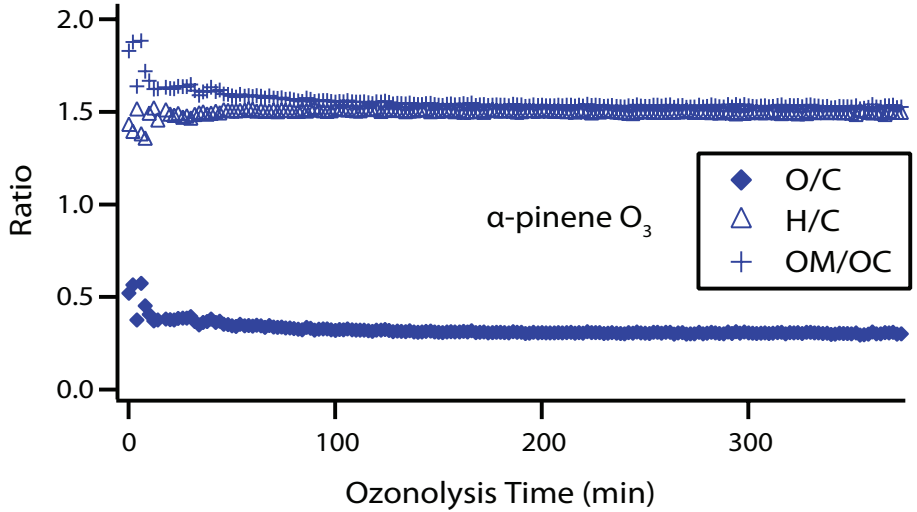

Fig. 3. O/C, H/C and OM/OC ratios for a typical α-pinene ozonolysis experiment (Experiment 4).

ACPD
9, 27485–27542, 2009

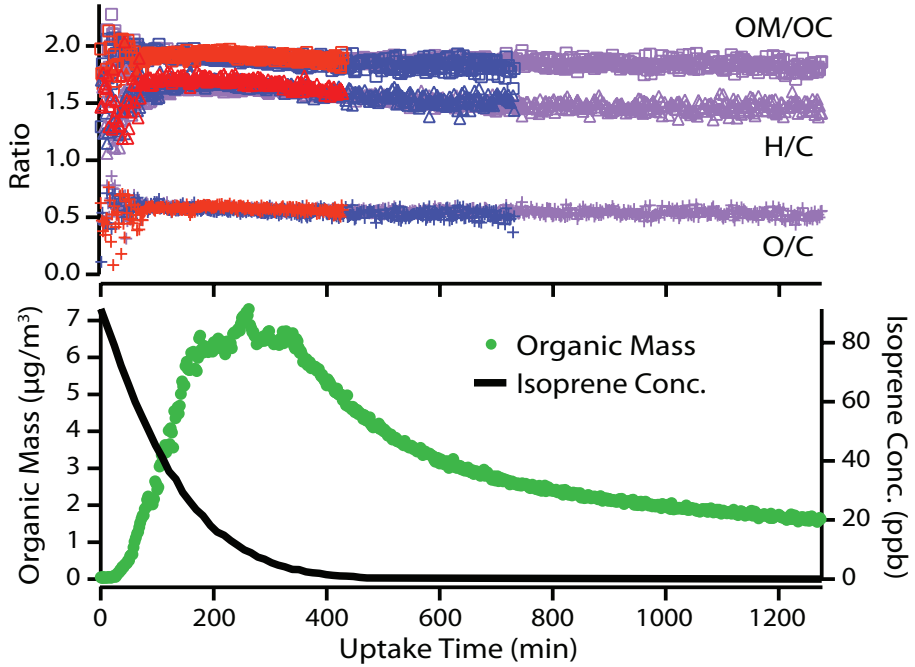

Fig. 4. Top Panel: O/C, H/C and OM/OC ratios of isoprene SOA formed under low-NO_x conditions. Experiment 8 is in blue, 9 in red, and 10 in purple. Bottom Panel: AMS organic mass loading (not corrected for collection efficiency) and isoprene concentration profile for Experiment 10.

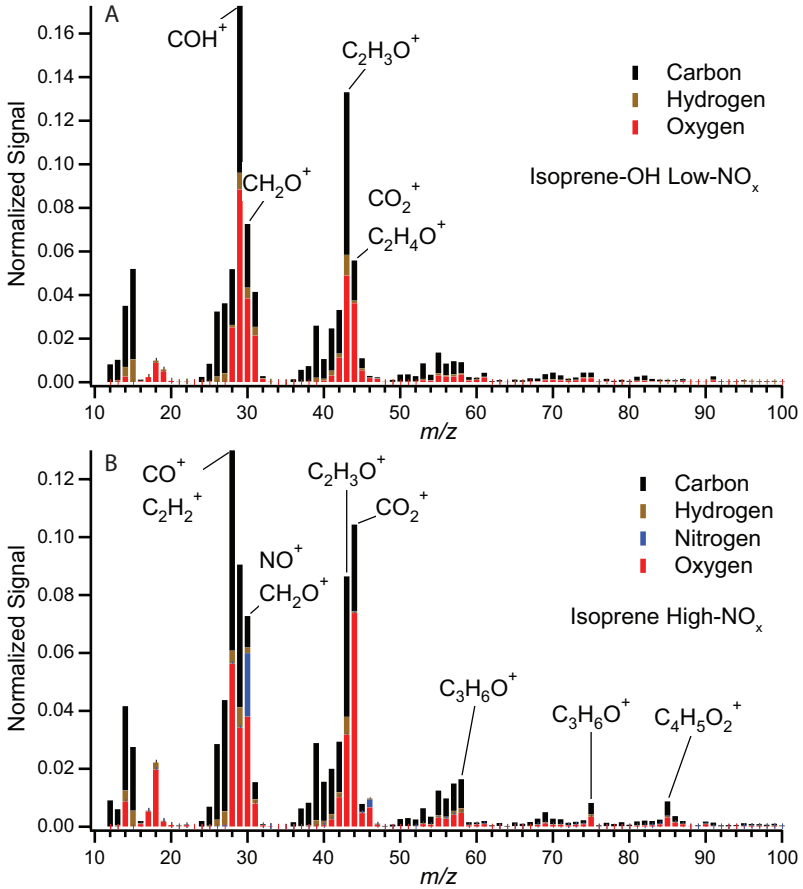

Fig. 5. High-resolution mass spectra of isoprene SOA formed under low-NO_x **(A)** and high-NO_x **(B)** conditions with elemental contributions to each mass-to-charge ratio shown. Spectra are taken at the peak of SOA growth.

ACPD
9, 27485–27542, 2009

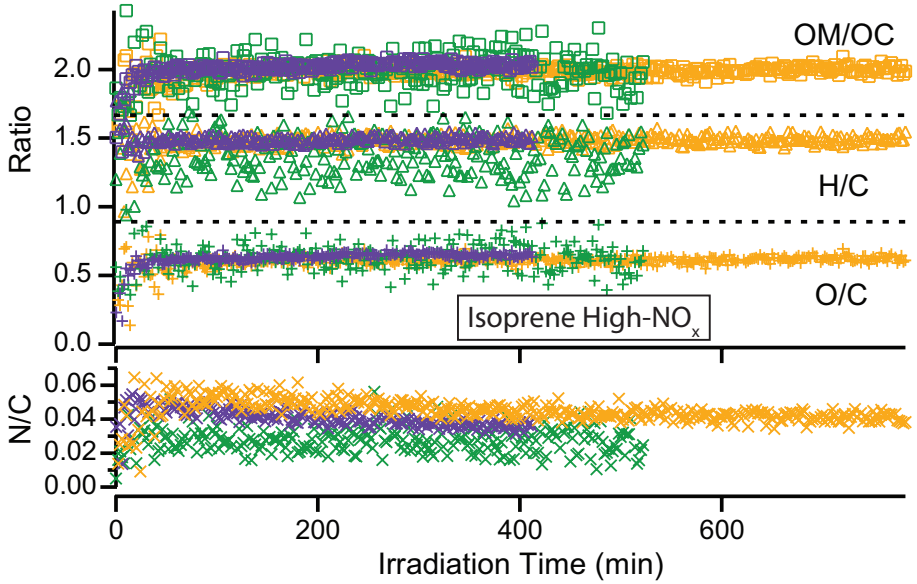

Fig. 6. Elemental ratios and OM/OC for isoprene high-NO_x experiments. Experiment 11 is in green, 12 in purple, and 13 in orange. Dotted lines are provided to visually separate different ratios.

ACPD
9, 27485–27542, 2009

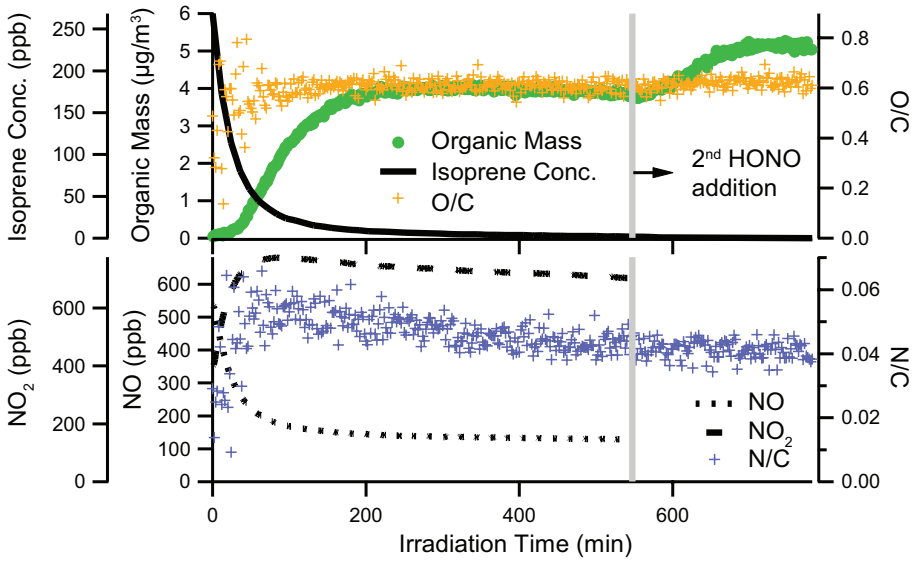

Fig. 7. Top panel: Time dependence of AMS organic mass (not corrected for collection efficiency), O/C ratio, and isoprene concentration for Experiment 12. Bottom panel: Time dependence of NO, NO_2, and N/C ratio for Experiment 12. A second addition of HONO at about 550 min after the start of the experiment is marked.

ACPD
9, 27485–27542, 2009

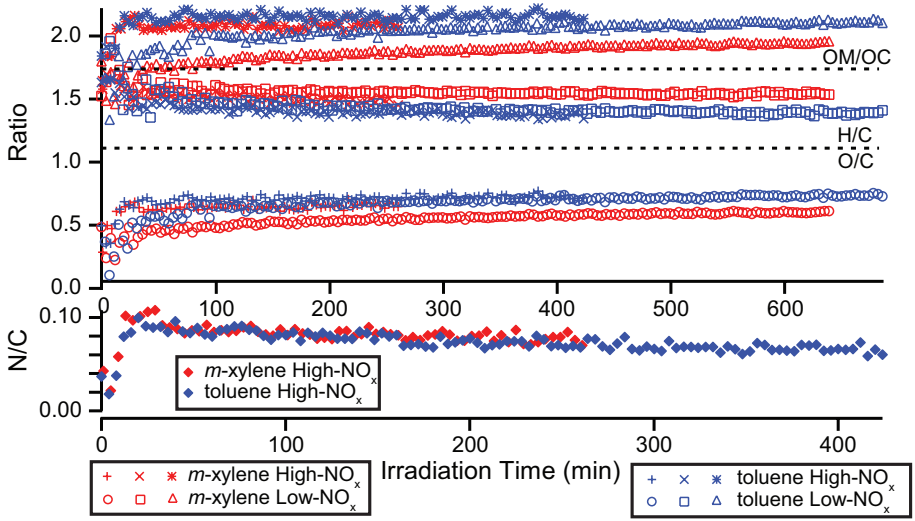

Fig. 8. Elemental ratios and OM/OC for single-ring aromatic experiments. Dotted lines are provided to visually separate different ratios.

ACPD
9, 27485–27542, 2009

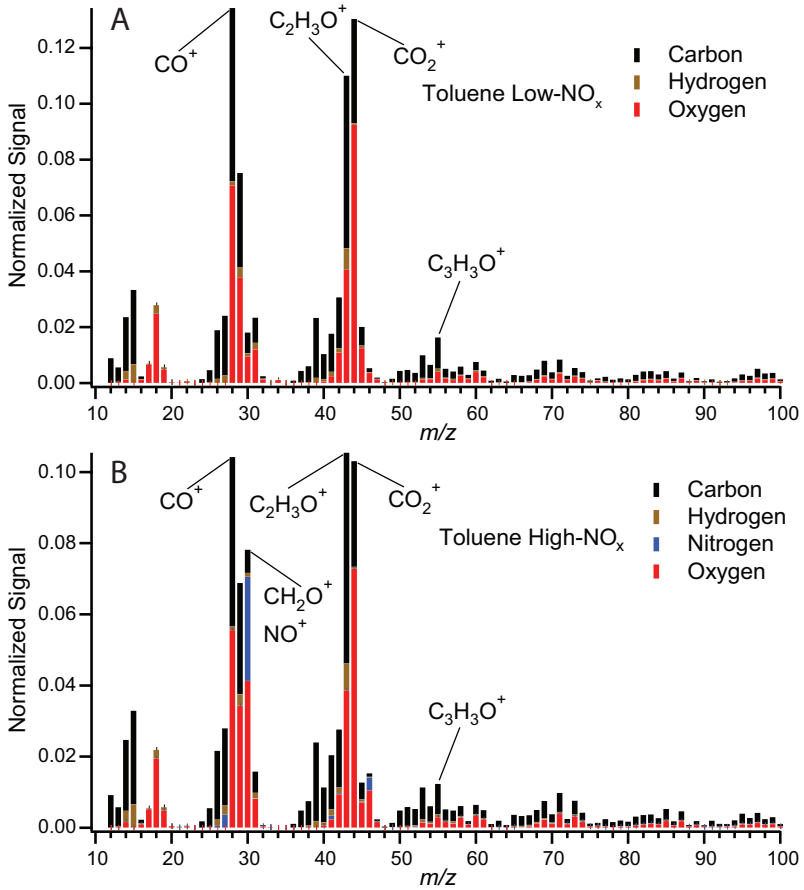

Fig. 9. High-resolution mass spectra of toluene SOA formed under low-NO_x **(A)** and high-NO_x **(B)** conditions with elemental contributions to each mass-to-charge ratio shown. Spectra are taken at the peak of SOA growth.

ACPD
9, 27485–27542, 2009

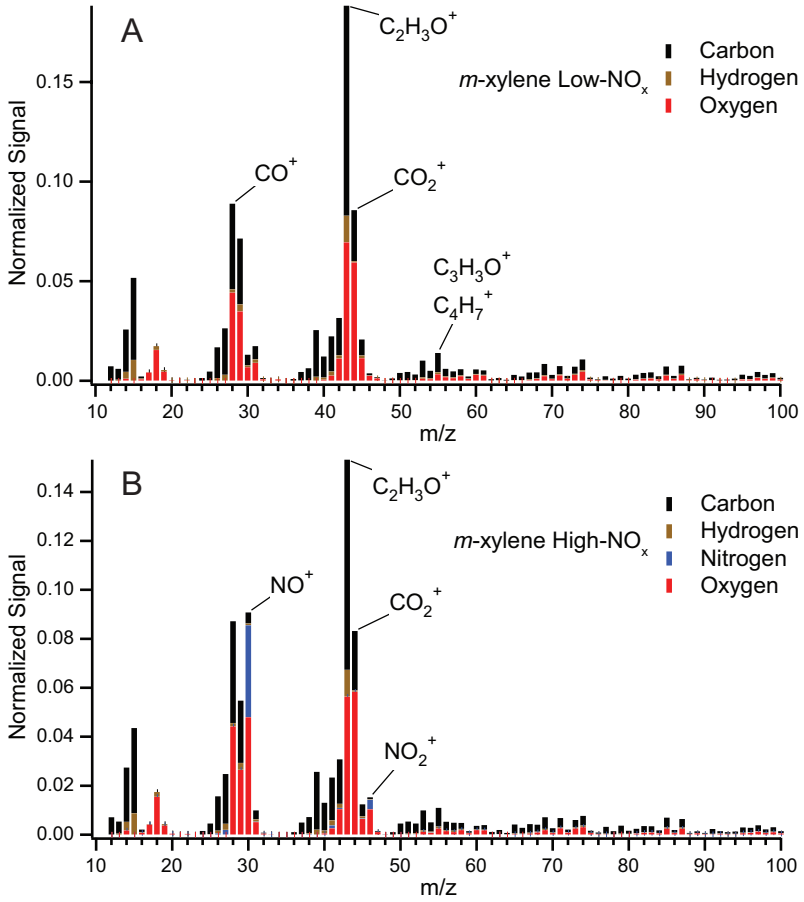

Fig. 10. High-resolution mass spectra of *m*-xylene SOA formed under low-NO_x **(A)** and high-NO_x **(B)** conditions with elemental contributions to each mass-to-charge ratio shown. Spectra were taken at the peak of SOA growth.

ACPD
9, 27485–27542, 2009

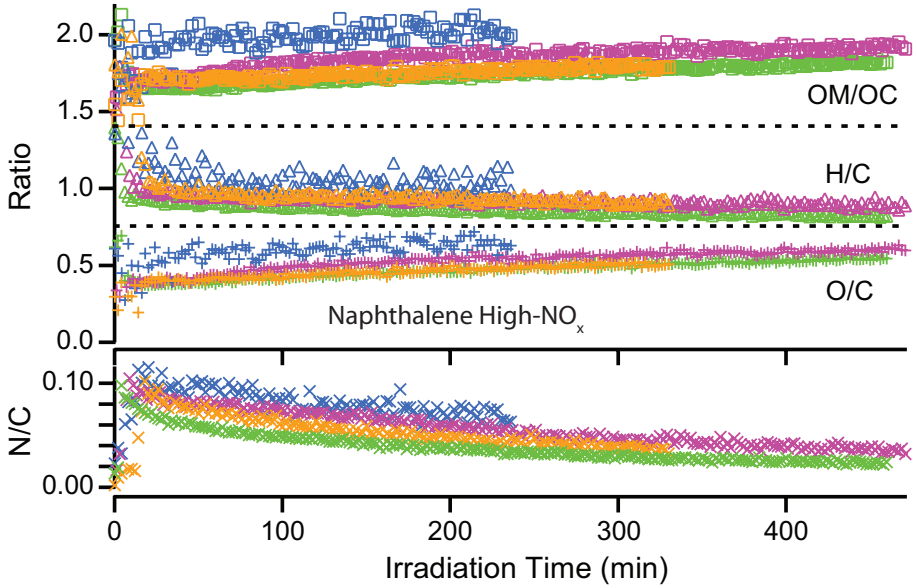

Fig. 11. Elemental ratios and OM/OC for naphthalene high-NO_x experiments. Experiment 23 is in blue, 24 in pink, 25 in orange and 26 in green. Dotted lines are provided to visually separate different ratios.

ACPD
9, 27485–27542, 2009

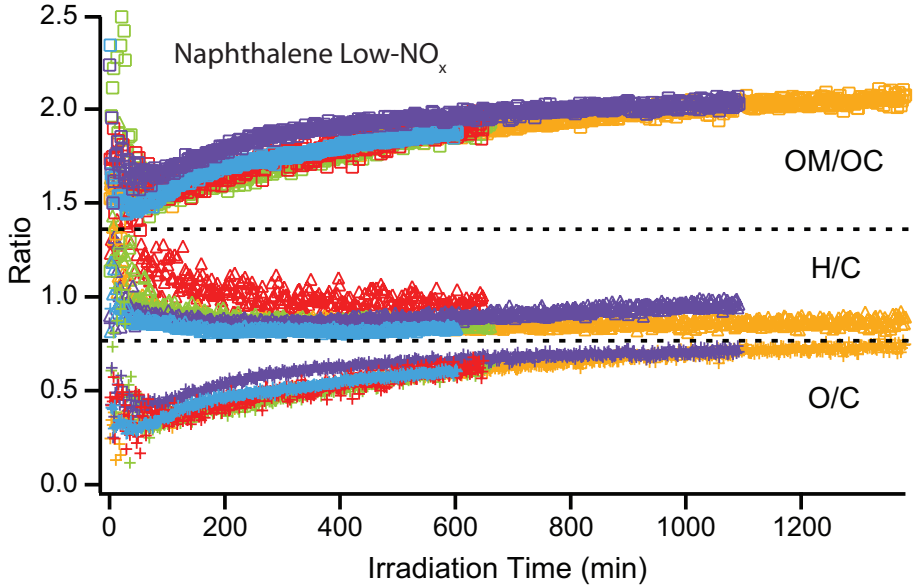

Fig. 12. Elemental ratios and OM/OC for naphthalene low-NO_x experiments. Experiment 18 is in red, 19 in purple, 20 in green, 21 in orange, and 22 in blue. Dotted lines are provided to visually separate different ratios.

ACPD
9, 27485–27542, 2009

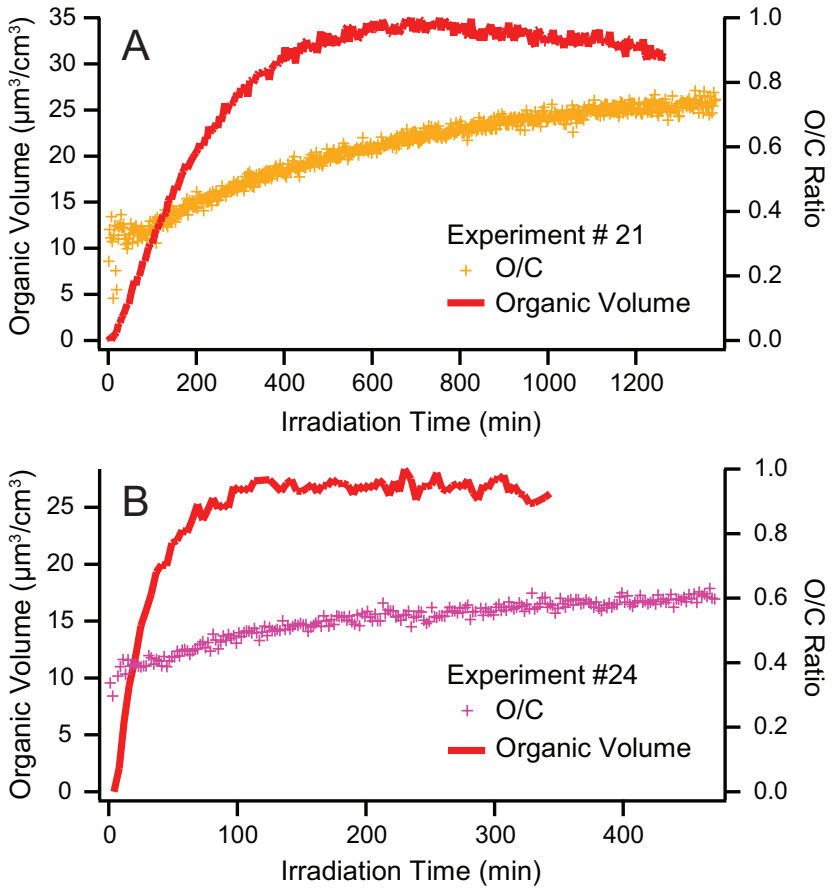

Fig. 13. Organic volume and O/C ratio as a function of time for typical naphthalene photooxidation experiments under low-NO_x (Experiment 21, **A**) and high-NO_x (Experiment 24, **B**) conditions.

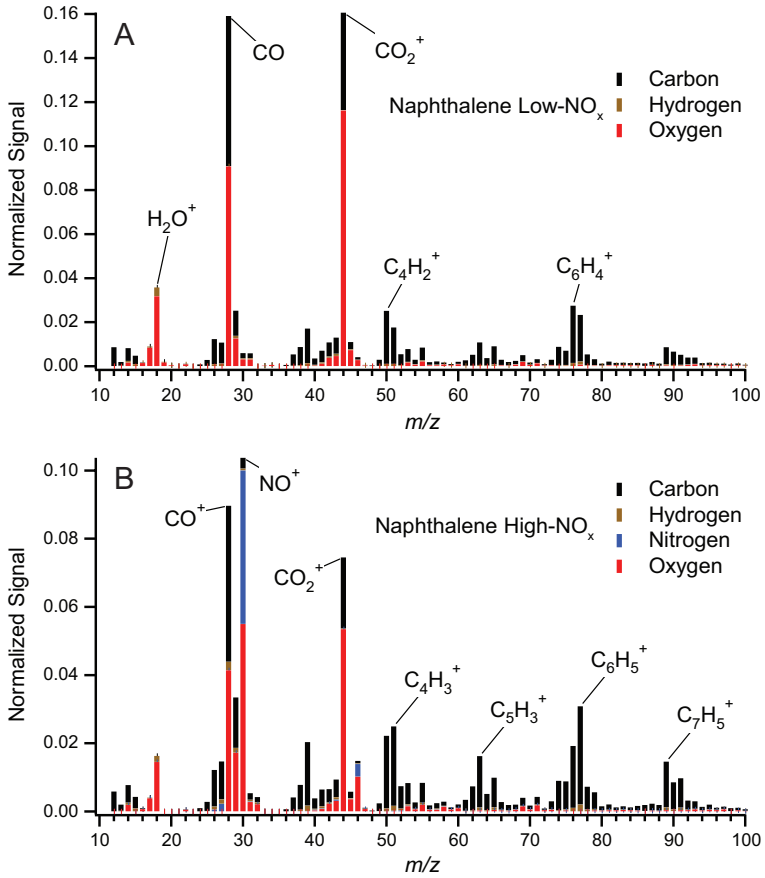

Fig. 14. High-resolution mass spectra of naphthalene-SOA formed under low-NO_x **(A)** and high-NO_x **(B)** conditions with elemental contributions to each mass-to-charge ratio shown. Spectra were taken at the peak of SOA growth.

ACPD
9, 27485–27542, 2009

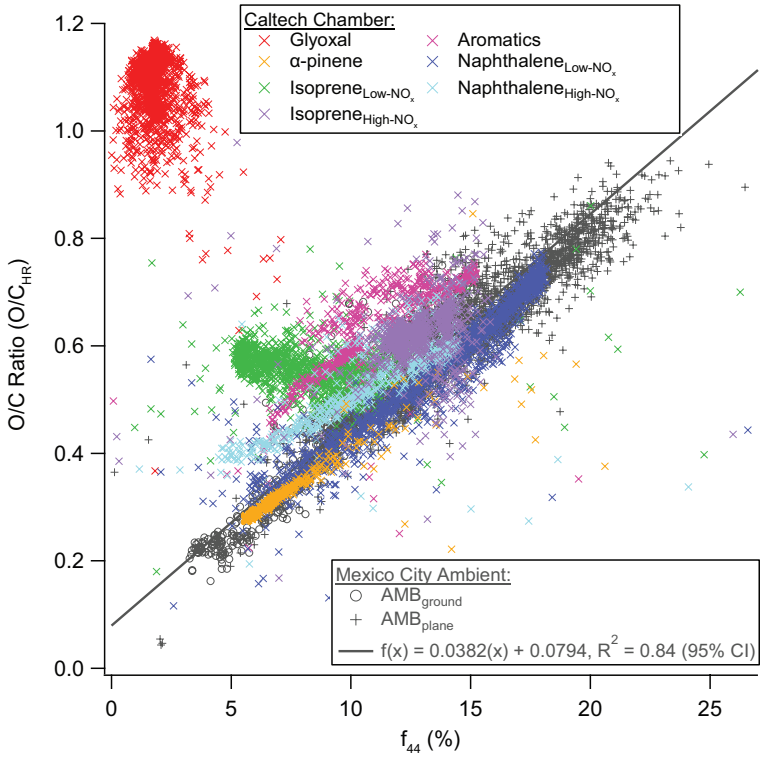

Fig. 15. O/C_{HR} vs. f_{44} for ambient Mexico City OA (Aiken et al., 2008, Fig. 4) and chamber OA. The solid line represents the correlation derived from ambient data. Experiments 19, 22, and 26 are not shown for simplicity.

ACPD
9, 27485–27542, 2009

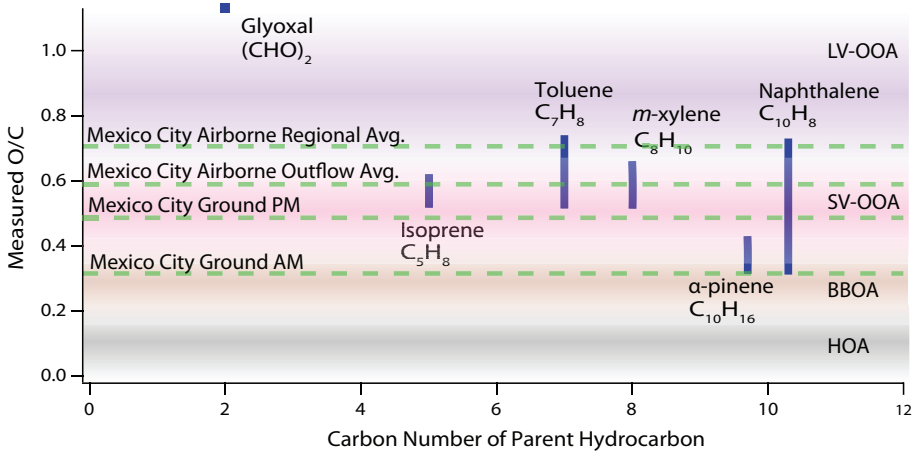

Fig. 16. O/C ratios for ambient Mexico City organic aerosol (Aiken et al., 2008), typical AMS components derived from positive matrix factorization (PMF) (Aiken et al., 2008, 2009; Ulbrich et al., 2009; Zhang et al., 2005b), and chamber SOA as a function of precursor carbon number. Ranges for each precursor represent the total O/C range achieved in the experiments surveyed here. Shaded regions represent the typically prescribed O/C ranges for AMS PMF components and can vary depending on the ambient data set.

ACPD
9, 27485–27542, 2009